Check for updates

Received: 6 June 2023 | Revised: 12 March 2024 | Accepted: 16 March 2024

DOI: 10.1002/dep2.282

The Depositional Record
Open Access
A journal of the International Association of Sedimentologists
WILEY

ORIGINAL RESEARCH ARTICLE

Tidal versus fluvial point bars: Key features from the integration of outcrop, core and wireline log information of Triassic examples

Luis Miguel Yeste[1] | **Marc Gil-Ortiz**[2] | **Fernando García-García**[1] | **César Viseras**[1] | **Neil David Mcdougall**[3] | **Patricia Cabello**[4] | **Luca Caracciolo**[5]

[1]Sedimentary Reservoirs Workgroup (SEDREGROUP), Department of Stratigraphy and Palaeontology, Facultad de Ciencias, S/N, 18003, University of Granada, Granada, Spain

[2]Departament de Mineralogia, Petrologia i Geologia Aplicada, UB-Geomodels, Facultat de Ciències de la Terra, Universitat de Barcelona, Barcelona, Spain

[3]Consultant Sedimentologist & Stratigrapher, Madrid, Spain

[4]Departament de Dinàmica de la Terra i de l'Oceà, UB-Geomodels, Facultat de Ciències de la Terra, Universitat de Barcelona, Barcelona, Spain

[5]Lehrstuhl für Geologie, GeoZentrum Nordbayern, Friedrich—Alexander Universität, Erlangen, Germany

Correspondence
Luis Miguel Yeste, Sedimentary Reservoirs Workgroup (SEDREGROUP), Department of Stratigraphy and Palaeontology, Facultad de Ciencias, S/N, 18003, University of Granada, Granada, Spain.
Email: lmyeste@ugr.es

Funding information
Ministerio de Universidades; Ministerio de Ciencia e Innovación, Grant/Award Number: PID2022-140850OB-C21 and PID2022-140850OB-C22

Abstract

The Triassic red beds of the Tabular Cover of the Iberian Meseta are an excellent reservoir outcrop analogue, a direct consequence of high-quality exposures, which offer exceptional three-dimensional outcrops, as well as a wide variability of depositional environments. Fluvial and transitional with tide-influenced and wave-influenced settings are recognised. Three point bar geobodies of similar scale, but influenced by different processes, were selected from this succession. Point bar geobody 1 was influenced by purely fluvial processes while geobodies 2 and 3 were tide-influenced. Both types of geobody were developed as point bar deposits in sinuous channels. A fully integrated study was carried out on these geobodies, utilising both outcrop and subsurface-based approaches, to characterise the key differences between fluvial and tidal point bars in the sedimentary record. The outcrop-based component involved traditional field data collection methods alongside digital techniques and data capture, including the use of digital outcrop models. Additionally, subsurface-based methods were employed, utilising core and wireline logs obtained from wells drilled in close proximity to the outcrop. The integration of these approaches aims to accurately differentiate the depositional settings of the three different geobodies, which while apparently very similar in many key respects also exhibit considerable differences when considered from the perspective of subsurface management of potentially similar geobodies. This study also emphasises the need to clearly distinguish high-sinuosity deposits based on their depositional sub-environment in order to properly evaluate their potential for subsurface management. Additionally, it highlights the presence and importance of internal baffles that may well influence fluid migration and indeed even compartmentalise geobodies. Three point bar geobodies of similar scale, but influenced by different processes, have been selected in this succession. A fully integrated study was carried out on these geobodies, utilising both

This is an open access article under the terms of the Creative Commons Attribution License, which permits use, distribution and reproduction in any medium, provided the original work is properly cited.
© 2024 The Authors. *The Depositional Record* published by John Wiley & Sons Ltd on behalf of International Association of Sedimentologists.

outcrop-based and subsurface-based approaches, to characterise the key differences between fluvial and tidal point bars in the sedimentary record.

KEYWORDS

fluvial point bar, outcrop analogue, outcrop/behind-outcrop characterisation, TIBEM, tidal point bar, Triassic

1 | INTRODUCTION

Following models of modern coastal depositional environments, mostly defined by Boyd et al. (1992) and Dalrymple et al. (1992), when the ratio between sediment supply and accommodation is high, river deposition dominates over marine redistribution and deltas typically form elongate/lobate shorelines. In contrast, during periods characterised by an excess of accommodation over sediment supply, embayed river palaeovalleys are transgressed to become estuaries, which form during relative sea-level rise. These depositional environments are extremely sensitive to not only changes in sea level but also climate and sediment supply (Blum et al., 2002; Anderson et al., 2023). Depending on whether coastlines are in regression or transgression, rivers on the coastal plain will typically experience varying degrees of interaction with the two main factors controlling sedimentation along shorelines, waves and tides (Olariu & Battacharya, 2006; Posamentier & Walker, 2006; Olariu et al., 2012; James & Dalrymple, 2010).

Shallow to marginal marine, tide-dominated environments are typically represented by mixed sand-prone and mud-prone systems restricted to estuaries, open coast tidal flats or tide-dominated deltas (Boyd et al., 1992; Harris et al., 2002; Harris & Heap, 2003; Dalrymple & Choi, 2007; Dashtgard et al., 2009; Dalrymple et al., 1992, 2012, 2015; Desjardins et al., 2012).

The combined effect of fluvial currents and tides becomes a highly efficient system of sediment sorting associated with the accumulation of sand-prone deposits in nearshore settings, either in shallow marine or in coastal plain marginal marine settings (Gil-Ortiz et al., 2019, 2022). The impact of sea-level variations and sediment supply may also result in significant variability in both stratigraphic architecture and sedimentological heterogeneity (Davis & Dalrymple, 2012; Ashworth et al., 2015; Tessier & Reynaud, 2016).

The interaction between tidal and river currents is a common feature in most marine basins. The extent of this zone of interaction depends on several factors, mainly including coastal plain gradient, tidal range at the coast and fluvial discharge (Dalrymple et al., 2015). The understanding of depositional processes in this fluvial to tidal transition has been a significant focus of study during the last few decades (Allen, 1991; Cuevas Gozalo & De Boer, 1991; Ghosh et al., 2005; Dalrymple & Choi, 2007; Van den Berg et al., 2007; Fischbein et al., 2009; Martinius & Gowland, 2011; Martinius & Van den Berg, 2011; Sisulak & Dashtgard, 2012; La Croix & Dashtgard, 2014; Jablonski & Dalrymple, 2016) although several key aspects are still poorly understood.

One such aspect is the characterisation of meandering fluvio-tidal channels. These have been much studied (Fustic et al., 2012; Carling et al., 2015; Dashtgard & La Croix, 2015; Díez-Canseco et al., 2015; Keevil et al., 2015) due to their complexity and similarity with pure fluvial high-sinuosity fluvial deposits (i.e. lateral accretion surfaces, inclined heterolithic stratification [IHS] and channel infill fining-upward profile). In order to differentiate between these, some key sedimentological trends must be carefully studied. These include (1) total mud volume together with the frequency and thickness of mud beds, (2) grain-size distribution on bars from upstream to downstream and (3) the cyclicity of bedding (Dashtgard & La Croix, 2015). In addition, trace fossil data can also substantially help to frame these deposits either in a continental fluvial or in a fluvio-tidal depositional environment (MacEachern & Pemberton, 1994; Pearson & Gingras, 2006; Gingras et al., 2016; Hayes et al., 2018; Melnyk & Gingras, 2020).

Fluvial and transitional deltaic/estuarine deposits are notably different in terms of reservoir heterogeneity, spatial distribution and fluid flow behaviour, so complexities become apparent when reservoir types are characterised for subsurface management, either for oil and gas exploration and production or, more recently, for CO_2 injection and storage (Chadwick et al., 2004; Zweigel et al., 2004; Ambrose et al., 2008; Pham et al., 2013; Issautier et al., 2014, 2016; Gershenzon et al., 2015, 2017; Al-Khdheeawi et al., 2017, 2018; Soltanian, et al., 2019; Sun et al., 2023).

The aim of this study was the characterisation of the key differences between fluvial and tidal point bars based on a Triassic succession located in the Iberian Meseta (Henares et al., 2014, 2016; Viseras et al., 2018; Yeste et al., 2019, 2020, 2021), in order to provide insight and

20554877, 0, Downloaded from https://onlinelibrary.wiley.com/doi/10.1002/dep2.282 by Readcube (Labtiva Inc.), Wiley Online Library on [14/05/2024]. See the Terms and Conditions (https://onlinelibrary.wiley.com/terms-and-conditions) on Wiley Online Library for rules of use; OA articles are governed by the applicable Creative Commons License

properly characterise and distinguish these deposits for subsurface resource management.

2 | GEOLOGICAL SETTING

The extensive Triassic Red Bed succession of the Iberian Meseta in south-central Spain, referred to as the TIBEM (Viseras et al., 2011, 2018; Henares et al., 2014, 2016; Yeste et al., 2019, 2020, 2021), is a continental deposit that accumulated during the Tethyan rifting process (Late Permian–Upper Triassic; López-Gómez et al., 2019). The study area, located east of Alcaraz (Albacete Province), corresponds to the most distal part of the TIBEM outcrop, as suggested by palaeocurrent data (Figure 1A; Fernández & Dabrio, 1985; Henares et al., 2014). Therefore, the TIBEM succession in the study area comprises fluvial to coastal deposits within a linked stratigraphic framework.

In the study area, the *ca* 160 m thick sedimentary succession (Ladinian-Norian) is divided into four informal member-rank lithostratigraphic units (Yeste et al., 2019). From the base to the top, they are (Figure 1B): (i) a mudstone–sandstone unit (M-S Unit) that includes both a meandering channel system and overbank sandstone deposits embedded in distal floodplain mudstones (Yeste et al., 2020); (ii) a sandstone unit (S Unit) corresponding to a braided system (Yeste et al., 2019); (iii) a heterolithic unit (H Unit) comprising alternating sandstone and mudstone layers deposited in a fluvial–marine transition zone (García-García et al., 2017; Yeste et al., 2017); and (iv) a mudstone-evaporitic unit (M-E Unit) composed of silt-rich coastal plain facies and intertidal sabkha evaporites. Previous genetically interpreted divisions of the Triassic red bed sedimentary succession (Fernández & Dabrio, 1985; Arche & López-Gómez, 2014) are avoided here in order to facilitate stratigraphic description, focussed on the basis of lithology and sedimentological features.

Two outcrops of the Alcaraz succession were selected for this study (Figure 1B): (1) Outcrop 1, located in the M-S Unit and (2) Outcrop 2, located in the H Unit.

The M-S Unit, which is at least 90 m thick, occurs at the base of the studied stratigraphic succession. The lower boundary was not observed in either outcrop or subsurface data in the study area, although its onlap across Palaeozoic palaeorelief is observed in nearby outcrops.

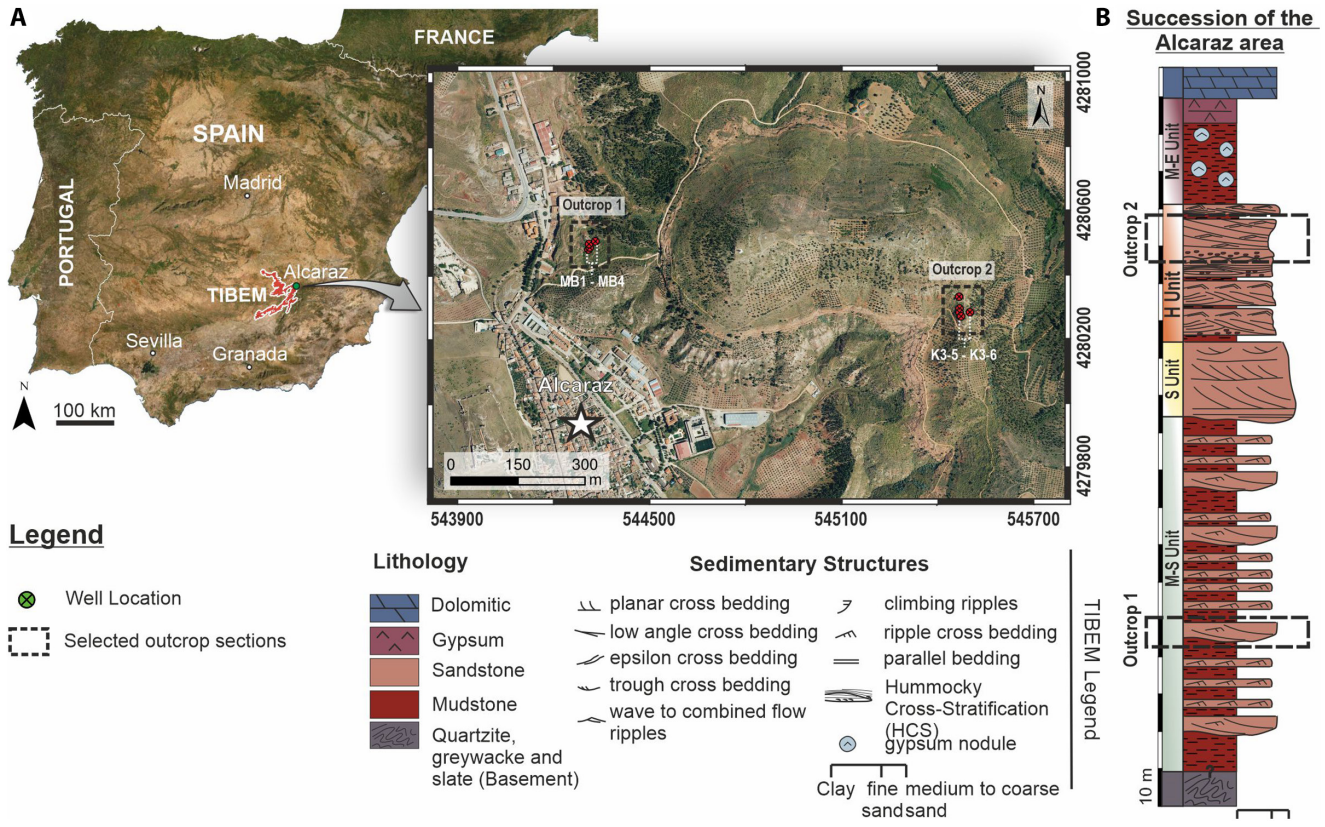

FIGURE 1 (A) Location of the study area (Alcaraz village, Albacete province, Spain) showing the location of the studied outcrops. Red points are well locations. Acronyms correspond to the well name. The rectangles indicate the position of the selected outcrop examples. (B) Synthetic stratigraphic succession of the selected study area (eastern of Alcaraz village). H Unit, Heterolithic Unit; M-E Unit, Mudstone-Evaporitic Unit; M-S Unit, Mudstone–Sandstone Unit; S Unit, Sandstone Unit. The rectangles indicate the position of the Mudstone–Sandstone Unit outcrop example and Heterolithic Unit outcrop example, selected for this study.

20554877, 0, Downloaded from https://onlinelibrary.wiley.com/doi/10.1002/dep2.282 by Readcube (Labtiva Inc.), Wiley Online Library on [14/05/2024]. See the Terms and Conditions (https://onlinelibrary.wiley.com/terms-and-conditions) on Wiley Online Library for rules of use; OA articles are governed by the applicable Creative Commons License

This unit is characterised by a low net-to-gross, effectively a sand: mud ratio of 10:90. It comprises lenticular, sand-prone packages up to 4 m thick, as well as thin, tabular, sand-prone packages, up to 2 m thick, encased within mud-prone sediments (Figure 1B). The main depositional environment is interpreted as a high-sinuosity fluvial system, characterised by meandering channels and associated overbank deposits (crevasse-splays) encased within argillaceous floodplain deposits (Yeste et al., 2020). An example of these high-sinuosity fluvial channels represented by Outcrop 1, located towards the lower part of the M-S Unit at the Alcaraz succession, was selected for this study (Figure 1B).

The H Unit at the Alcaraz succession is 40 m thick, characterised by medium net-to-gross (sand: mud ratio of 60:40), comprising metre-scale heterolithic sandstone-dominated packages encased in mudstones (Figure 1B). Sediments were deposited in a fluvial–-marine transition zone interpreted as a mixed tidal and wave-influenced shoreline system (García-García et al., 2017; Yeste et al., 2017). An incised surface has been recognised towards the middle of the H Unit succession. This major stratigraphic surface is interpreted as an incised valley (García-García et al., 2017; Yeste et al., 2017). Confined within this incised valley, two sand-prone packages are described. Towards the base of the incised valley, the first sand-prone package is characterised by storm-dominated shoreface deposits (García-García et al., 2017). The top of this package is eroded by the second sand-prone package confined within the incised valley, characterised by a high-sinuosity tide-dominated system (Yeste et al., 2017), which was the selected example, Outcrop 2, for this study (Figure 1B).

3 | METHODS AND DATA

A multidisciplinary outcrop/behind-outcrop (OBO) characterisation workflow was applied in this study, including a detailed sedimentological description from both surface (outcrop-derived and digital outcrop-derived observations and measurements) and subsurface (cores and well logging) data (Figure 2).

Digital outcrop models (DOMs) have also been created from photogrammetry with a remotely piloted aircraft system (RPAS) to complete the outcrop-derived measurement dataset. The RPAS used was a multi-rotor octocopter with a Sony ILCE 6000 camera of 24 Mpx. For the DOM the professional software Agisoft PhotoScan$_{TM}$ was used, which was specifically designed for drone-based mapping.

Wells were drilled with continuous core recovery, and wireline log data were also obtained. Cores were slabbed to enhance the visibility of sedimentary features on the core surface and allow the identification of the main simple lithofacies classes (Table 1). Well log data include the total gamma ray log (GR) in addition to borehole imaging from Optical and Acoustic televiewers (OBI and ABI, respectively). The GR log provides total gamma radioactivity counts from U, Th and K in API units. The ABI is a slim-hole logging tool with an ultrasonic transducer sensor, which provides a 360° oriented acoustic image (amplitude and travel time). The OBI is also a slim-hole logging tool but with a high-sensitivity digital image sensor which provides a 360° RGB true colour-oriented image of the borehole wall. Dip tadpoles interpreted from the ABI and OBI, together with GR pattern analysis, provide information on the spatial distribution, orientation and dip of the main sedimentary surfaces and structures.

Two outcrops were selected to apply the OBO characterisation workflow, as previously described, based on their exceptional three-dimensional exposure and logistical ease for drilling behind the outcrop. Outcrop 1 includes geobody 1, while Outcrop 2 includes both geobodies 2 and 3.

In Outcrop 1, where geobody 1 is located, four slim-hole (6.25″ diameter), behind-outcrop wells allowed subsurface characterisation (Figure 1A). From south to north, these wells are MB1, with 4.6 m of core and well logging interval; MB2, with 1.9 m of core and well logging interval; MB3, with 4.8 m of core and well logging interval; and MB4, with 8 m of core and well logging interval.

In Outcrop 2, where geobodies 2 and 3 are located, six slim-hole (6.25″ diameter), behind-outcrop wells allowed subsurface characterisation by providing information from the wells and cored intervals (Figure 1A). From north to south, these wells are K3-1, with 7.55 m of core and well logging interval; K3-2, with 14.7 m of core and well logging interval; K3-3, with 9.8 m of core and well logging interval; K3-4, with 34.55 m of core and well logging interval; K3-5, with 15 m of core and well logging interval; and K3-6, with 35.6 m of core and well logging interval.

4 | RESULTS

Twelve lithofacies were identified in this study, and detailed descriptions of three point bar geobodies (Point bar geobodies 1–3), including lateral and vertical lithofacies variation, geometric data, bounding surfaces and the dimensions of the sedimentary bodies, from both outcrop and subsurface data, were used to characterise the spatial distribution of heterogeneities. Point bar geobody 1, drilled by Wells MB1 to MB4, is located at Outcrop 1. Point bar geobodies 2 and 3 are located at Outcrop 2, infilling the incised valley (Figure 1). Point bar geobody 2 was

20554877, 0, Downloaded from https://onlinelibrary.wiley.com/doi/10.1002/dep2.282 by Readcube (Labtiva Inc.), Wiley Online Library on [14/05/2024]. See the Terms and Conditions (https://onlinelibrary.wiley.com/terms-and-conditions) on Wiley Online Library for rules of use; OA articles are governed by the applicable Creative Commons License

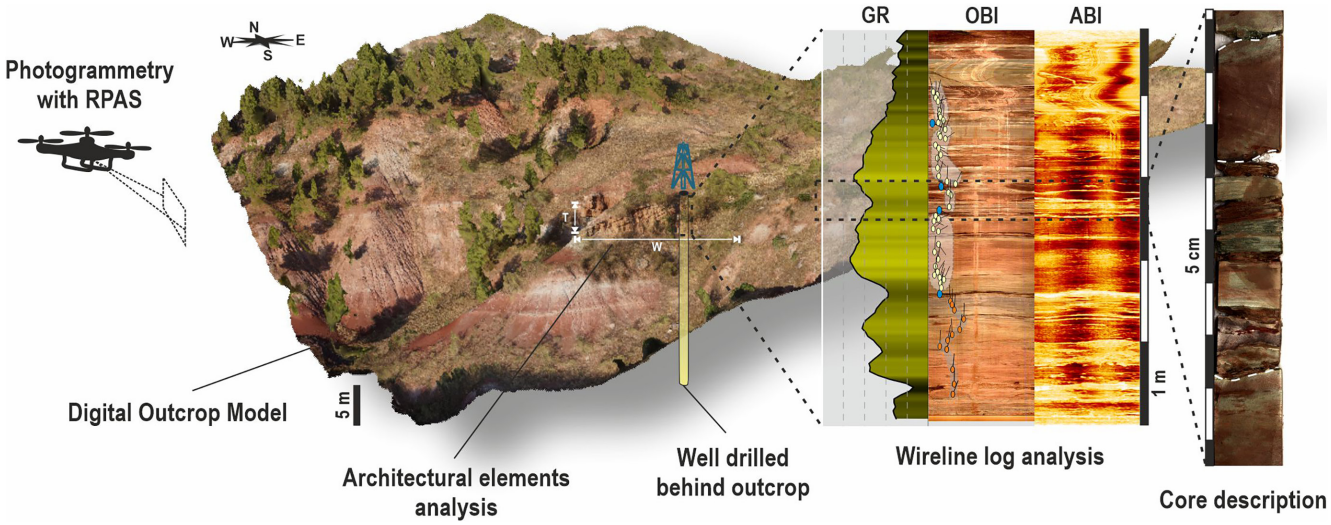

FIGURE 2 Outcrop/behind-outcrop (OBO) characterisation workflow designed and applied in this study including outcrop-derived and digital outcrop-derived observations and measurements, core description, gamma ray logging and borehole imaging logs. ABI, Acoustic televiewer log; GR, gamma ray log; OBI, Optical televiewer log; RPAS, remotely piloted aircraft system.

drilled by Wells K3-2 to K3-5, while Point bar geobody 3 was drilled by Wells K3-1 to K3-4.

4.1 | Lithofacies

Twelve lithofacies were classified mainly according to grain size and dominant sedimentary structures. The bioturbation index (BI) was also established using the Reineck scale (Reineck, 1963; Taylor & Goldring, 1993). These lithofacies are described and interpreted below. The sedimentological characteristics of the documented lithofacies are summarised in Table 1 and illustrated in Figure 3. The most relevant ichnotaxa are also illustrated with core examples in Figure 4.

4.1.1 | Lithofacies Gm: Conglomerate lag

Lithofacies Gm is composed mainly of sandy conglomerates dominated by pebble-sized mud clasts embedded in a medium-grained to very fine-grained sandstone matrix (Figure 3A). This lithofacies appears massive, with weak horizontal bedding or rare cross-bedding. Lithofacies Gm occurs as single beds, up to 20 cm thick, with an erosive base and is gradational into trough cross-bedded sandstone (Lithofacies St) and/or ripple cross-laminated sandstone (Lithofacies Sr). Mud clasts occur as bed parallel aligned and/or randomly oriented (Figure 3A), showing normal and inverse grading. Bioturbation is absent or not recognised in this lithofacies (BI 0).

The erosional base and poorly sorted clasts in a medium-grained to very fine-grained matrix indicate deposition under high-energy traction currents. The normal grading suggests rapid deposition from decelerating turbulent flows, whereas the inverse grading indicates dispersive pressure (Lowe, 1979), or deposition during a waxing flow stage (Ichaso & Dalrymple, 2014). Poorly sorted beds with a high matrix percentage might also indicate deposition from high-concentration sediment flows (Nemec & Steel, 1984) and/or rapid accumulation in a sandy setting (Ichaso & Dalrymple, 2014). The mud clasts are most probably derived from cut-bank caving and slumping and/or reworking of desiccated mud drapes previously deposited on the point bar (Thomas et al., 1987).

4.1.2 | Lithofacies Sm: Massive sandstone

Lithofacies Sm comprises massive beds of medium-grained sandstones without any apparent internal structure (Figure 3B). This lithofacies is characterised by good to moderate sorting with a sand: mud ratio of between 100:0 and 90:10. The thickness of single beds varies between 5 and 40 cm. Rarely, intraformational mudstone rip-up clasts are also present in this lithofacies (Figure 3B). Bioturbation is absent or not recognised in this lithofacies (BI 0).

These massive sandstones are interpreted as the deposits of short-lived mass flows which dumped sediments at a rate too fast for hydraulic sorting processes to work effectively (Smith, 1986; Hjellbakk, 1997). Such flood flows may develop by adding sediments to fast-flowing stream flows (Turner & Monro, 1987). The presence of intraformational mudstone rip-up clasts indicates relative short transport distance for the sediments (Hjellbakk, 1997).

20554877, 0, Downloaded from https://onlinelibrary.wiley.com/doi/10.1002/dep2.282 by Readcube (Labtiva Inc.), Wiley Online Library on [14/05/2024]. See the Terms and Conditions (https://onlinelibrary.wiley.com/terms-and-conditions) on Wiley Online Library for rules of use; OA articles are governed by the applicable Creative Commons License

TABLE 1 Lithofacies identified in this study. See Figure 3 for photographic examples of each lithofacies.

Code	Texture and fabric	Sedimentary structures and characteristics	Main process/interpretation
Gm	Pebble-cobble. Clast or matrix supported	Massive, weak horizontal bedding or planar cross-bedding. Erosive base and mud rip-up clasts	Associated with high-energy traction current
Sm	Fine to medium sand	Massive. Rarely, presence of mud clasts	Associated with rapid transport and deposition of sand during major floods
Sh	Fine to medium sand	Horizontal lamination. Occasionally presence of mud drape and flame structures	Associated with upper flow regime deposition
St	Fine to medium sand	Trough cross-bedding. Sometimes, mud chips lining the cross-beds	Migration of megaripples and dunes. Moderate to strong river and tide-influenced currents
Sr	Very fine to fine sand	Current ripple lamination. Presence of occasional *Arenicolites* and *Taenidium* burrows	Migration of current ripples. Associated with moderate to strong river and tide-influenced currents
Sw	Very fine to fine sand	Wave ripple lamination. Presence of occasional *Planolites and Thalassinoides* burrows	Oscillatory flow during both fair weather and storm events
Sb	Very fine to medium sand	Massive. Presence of rhizoliths, *Arenicolites*, *Planolites*, *Taenidium* and *Thalassinoides* burrows	Structureless due to bioturbation
HS	Very fine sand to fine sandstone	Flaser bedding. Sand alternates with minor mud drapes	Tide-influenced unidirectional currents with low to moderate speeds. Alternation of low and high energy conditions. Sandy ripples were deposited by high energy tidal and/or fluvial flows, while muddy drapes were deposited during slack water conditions
HSi	Very fine sand to silt and clay	Heterolithic trough cross-bedding. Presence of sand–mud couplets forming bundles. Rarely, presence of mud clasts and convolute lamination	Tide-influenced unidirectional currents with moderate speeds. Sand bedsets are formed by tidal currents. Mud drapes are formed during the low energy periods of slack water
HMi	Very fine sand to silt and clay	Inclined heterolithic bedding. Frequent presence of slumped layers. Presence of occasional *Arenicolites* and *Taenidium* burrows	Tide-influenced unidirectional currents with moderate speeds, whereas the mud layers accumulated from suspension under low energy, slack water conditions
HM	Very fine sand to silt and clay	Wavy and lenticular bedding. Roughly equal volumes of sand and mud. Current, wave and/or combined-flow ripples are also present. Presence of occasional *Arenicolites* and *Thalassinoides* burrows	Tide-influenced unidirectional currents with low to moderate speeds. Alternation of low and high energy conditions. Sandy ripples were deposited by high energy tidal and/or fluvial flows, while muddy drapes were deposited during slack water conditions
Fm	Clay	Massive to horizontal lamination (lower flow regime). Presence of rhizoliths. Intense bioturbation, including scattered *Taenidium* burrows	Settling from suspension in very low energy conditions

4.1.3 | Lithofacies Sh: Parallel-laminated sandstone

Lithofacies Sh consists predominantly of horizontal to low-angle (<10°) parallel-laminated fine-grained to very fine-grained sandstones (Figure 3C). This lithofacies is characterised by good to moderate sorting with a sand:mud ratio varying between 100:0 and 80:20. The horizontal-laminated sandstones occur as single beds, from 0.1 to 1.2 m thick. Rarely, flame structures are also present (Figure 3C). Bioturbation is not recognised in this lithofacies (BI 0).

This facies is interpreted as an upper flow regime deposit, formed during flood conditions (Miall, 1992; Broughton, 2016; Gil-Ortiz et al., 2019; Yeste et al., 2020). The well-laminated sandstones indicate a high degree of hydrodynamic sorting, directly related to flow intensity and particle-by-particle bed erosion (Simons et al., 1965). Flame structures are caused by squeezing of low-density, water-saturated muds upward into denser sand layers owing to the weight of the sand, the density difference and speed of deposition (Collinson &Thompson, 1989).

20554877, 0, Downloaded from https://onlinelibrary.wiley.com/doi/10.1002/dep2.282 by Readcube (Labtiva Inc.), Wiley Online Library on [14/05/2024]. See the Terms and Conditions (https://onlinelibrary.wiley.com/terms-and-conditions) on Wiley Online Library for rules of use; OA articles are governed by the applicable Creative Commons License

4.1.4 | Lithofacies St: Trough cross-bedded sandstone

Lithofacies St comprises medium-grained to very fine-grained, trough cross-bedded sandstones (Figure 3D). This lithofacies shows good to moderate sorting and sand:mud ratios of between 100:0 and 90:10. Lithofacies St occurs as fining-upward cosets up to 1 m thick (the thickness of single beds varies between 0.1 m to 1 m), with sharp or erosive base (Figure 3D). Locally, mud drapes and mudstone intraclasts line set bases and foresets (Figure 3D). Less commonly, this facies is overlain by ripple cross-laminated sandstones (Lithofacies Sr) or sandy inclined-bedded heterolithic sandstone (Lithofacies HSi). Bioturbation is absent or not recognised in this lithofacies (BI 0).

This lithofacies is interpreted as a channel fill of sinuous crested dunes migrating under fluvial or tidal currents, reflecting a moderate to strong energy regime (Collison

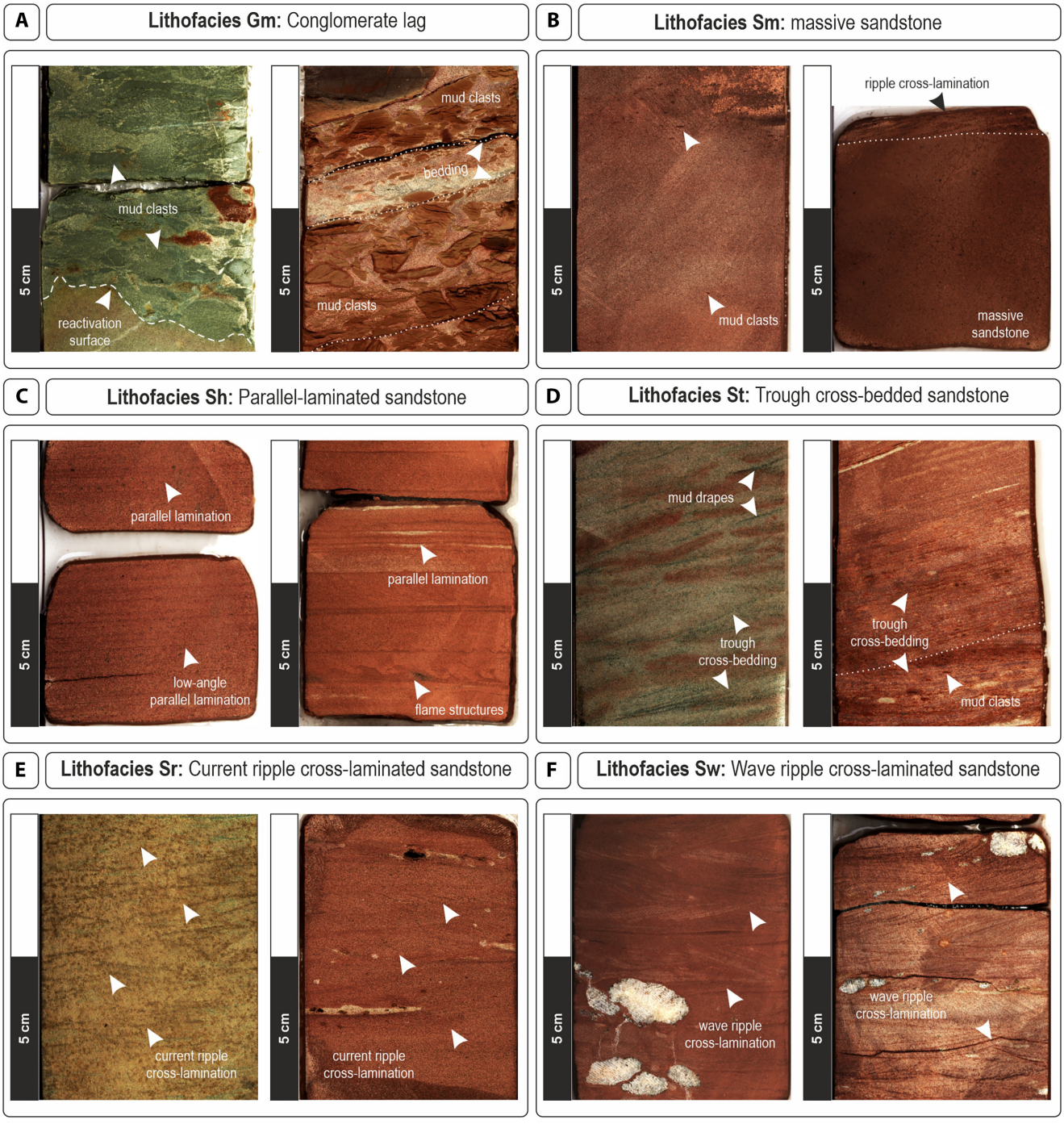

FIGURE 3 Typical examples of lithofacies identified in this study from slabbed cores.

20554877, 0, Downloaded from https://onlinelibrary.wiley.com/doi/10.1002/dep2.282 by Readcube (Labtiva Inc.), Wiley Online Library on [14/05/2024]. See the Terms and Conditions (https://onlinelibrary.wiley.com/terms-and-conditions) on Wiley Online Library for rules of use; OA articles are governed by the applicable Creative Commons License

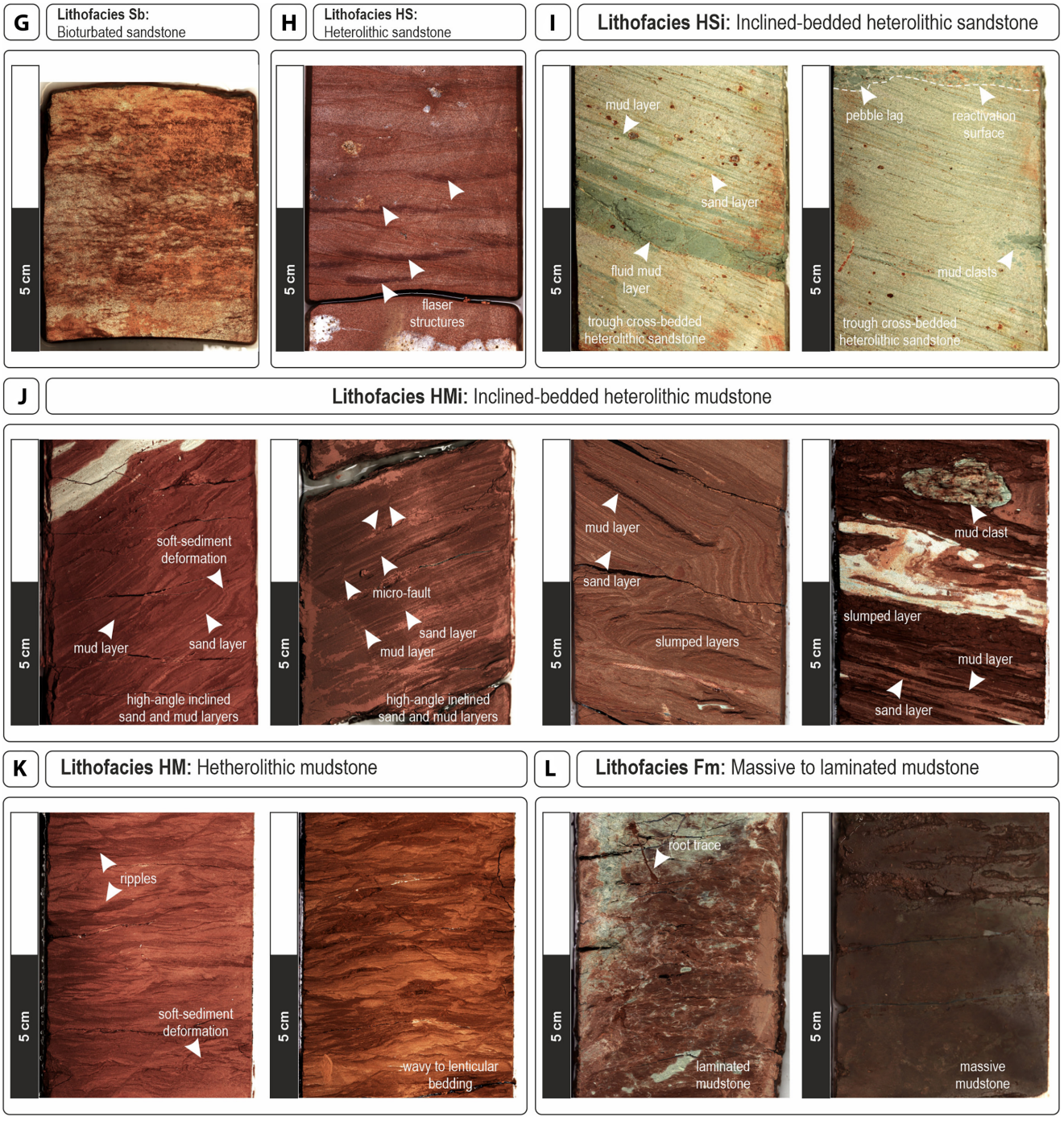

FIGURE 3 (Continued)

et al., 2006; Bradley et al., 2018; Viseras et al., 2018; Yeste et al., 2020).

4.1.5 | Lithofacies Sr: Current ripple cross-laminated sandstone

Lithofacies Sr consists of fine-grained to very fine-grained sandstones, characterised by asymmetrical ripple marks and gently inclined cross-lamination (Figure 3E). This lithofacies shows poor to moderate sorting with a sand:mud ratio varying between 100:0 and 90:10. Lithofacies Sr appears as individual sets with a thickness that varies from around 2 to 5 cm and beds up to 40 cm thick. Bioturbation is absent to sparse with only the presence of occasional *Arenicolites*, *Taenidium* and indeterminate horizontal burrows (BI 0–1).

Lithofacies Sr is attributed to the downcurrent migration of sinuous trains of asymmetrical ripples, deposited under a low to moderate flow regime (Allen, 1963; Miall, 1996).

20554877, 0, Downloaded from https://onlinelibrary.wiley.com/doi/10.1002/dep2.282 by Readcube (Labtiva Inc.), Wiley Online Library on [14/05/2024]. See the Terms and Conditions (https://onlinelibrary.wiley.com/terms-and-conditions) on Wiley Online Library for rules of use; OA articles are governed by the applicable Creative Commons License

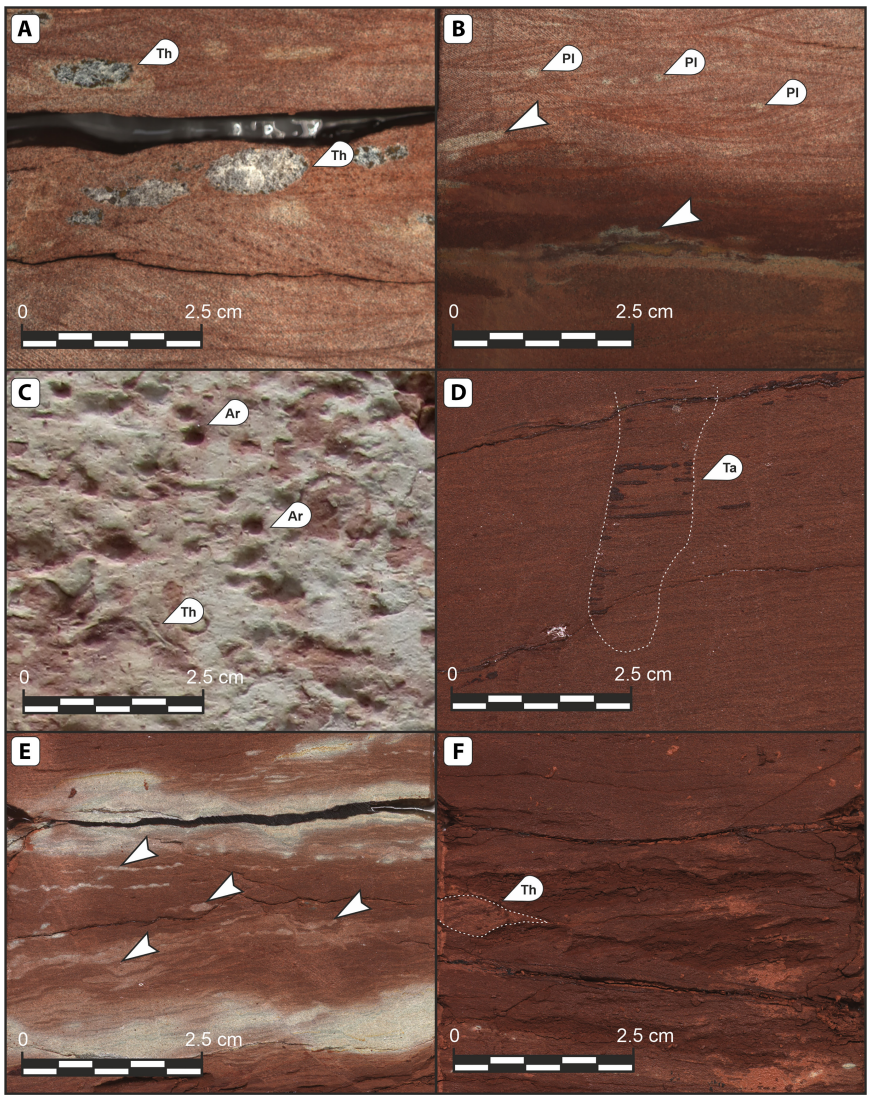

FIGURE 4 Ichnotaxa identified in these deposits with characteristic low-diversity ichnofacies. (A) Wave ripple cross-laminated sandstones with scattered large *Thalassinoides* burrows filled with gypsum. (B) Wave ripple cross-laminated sandstones with *Planolites* and horizontal indeterminate burrows. (C) Plan view of outcropping bioturbated sandstones with characteristic *Arenicolites* and *Thalassinoides* burrows. (D) Inclined-bedded heterolithic mudstones with a *Taenidium* burrow. (E) Inclined-bedded heterolithic mudstones with low to moderate bioturbation with scattered indeterminate horizontal burrows. (F) Heterolithic mudstones with a Thalassionides burrow. Ar, *Arenicolites*; Pl, *Planolites*; Ta, *Taenidium*; Th, *Thalassinoides*.

4.1.6 | Lithofacies Sw: Wave ripple cross-laminated sandstone

Lithofacies Sw consists of fine-grained to very fine-grained sandstones, characterised by asymmetrical wave ripple cross-lamination (Figure 3F). This lithofacies is also characterised by moderately to well-sorted sandstones and sand:mud ratios varying between 100:0 and 90:10. Lithofacies Sw appears as individual sets with a thickness varying from 2 to 5 cm and beds up to 40 cm thick. Bioturbation is absent to sparse characterised by only low to very low-diversity assemblages of *Thalassinoides* (Figure 4A), *Planolites* and indeterminate horizontal burrows (Figure 4B) (BI 0–1).

This facies shows evidence for combined flow conditions, with a dominant unidirectional component and a superimposed oscillatory motion due to wind-driven residual motion and/or tidal currents (Hill et al., 2003; Yang et al., 2005; Ichaso & Dalrymple, 2014).

4.1.7 | Lithofacies Sb: Bioturbated sandstone

The bioturbated sandstone lithofacies (Sb) comprises poorly sorted, fine to very fine-grained sandstones, 0.1 to 0.5 m thick, often moderately to heavily bioturbated (BI 4–6). The most characteristic ichnotaxa identified include *Arenicolites*, *Planolites*, *Taenidium* and *Thalassinoides* (Figure 4C). Rhizoliths, mottling and indeterminate horizontal burrows also occur. Primary sedimentary structures are often entirely obliterated, although cross-bedding, ripple cross-lamination or parallel-lamination are locally preserved (Figure 3G). Rare scattered granule-sized clasts are also present.

The fine-grained sandstones, showing common to abundant bioturbation dominated by a horizontal, deposit-feeding, low-diversity *Cruziana* and mixed *Mermia-Scoyenia* ichnofacies (Diéz-Canseco et al., 2015), coupled with locally preserved current-dominated structures, suggest a low to moderate energy environment. This facies is

20554877, 0, Downloaded from https://onlinelibrary.wiley.com/doi/10.1002/dep2.282 by Readcube (Labtiva Inc.), Wiley Online Library on [14/05/2024]. See the Terms and Conditions (https://onlinelibrary.wiley.com/terms-and-conditions) on Wiley Online Library for rules of use; OA articles are governed by the applicable Creative Commons License

interpreted to record colonisation by fauna and flora in dominantly shallow freshwater environments, occasionally invaded by brackish waters during upstream tidal currents incursions and reduced sedimentation during slack water periods in a fluvial-to-tidal transition zone.

4.1.8 | Lithofacies HS: Heterolithic sandstone

Lithofacies HS is characterised by an interbedding of well to moderately sorted, fine to very fine-grained sandstones with thin mudstone drapes, with sand:mud ratios varying between 90:10 and 60:40. This lithofacies displays flaser structures together with combined current and wave ripple cross-lamination (Figure 3H). Bioturbation is sparse to low with only indeterminate horizontal burrows (BI 0–2).

Sandy ripples indicate deposition under high energy tidal and/or fluvial flows events, while the muddy drapes were deposited during slack water periods (Reineck & Wunderlich, 1968; Shanley et al., 1992).

4.1.9 | Lithofacies HSi: Inclined-bedded heterolithic sandstone

Lithofacies HSi comprises interbedded 0.1–0.6 m thick, fine to very fine-grained sandstone and mudstone, with sand:mud ratios varying between 90:10 and 60:40 (Figure 3I). This facies is characterised by low-angle to high-angle cross-bedding and trough cross-bedding, showing bipolarity in palaeoflow directions. Commonly, pebble lags are present, overlying reactivation surfaces and grading to very fine-grained sandstones (Figure 3I). In addition, fluid mud layers are also present in this facies (Figure 3I). Bioturbation is absent to sparse with only indeterminate horizontal burrows (BI 0–1).

The heterolithic nature, coupled with the presence of paired sandstone and mudstones, indicates that tidal currents played an important role in the deposition of this lithofacies. The presence of pebble lags showing normal grading into very-fine sandstone suggests that river floods were also important. Fluid mud layers are commonly associated with zones characterised by tidal processes and the mixing of fresh and salt water which trap the suspended sediment supplied by the river (turbidity maximum zone; Glangeaud, 1938; Postma & Kalle, 1955; Jay et al., 2015). Additionally, such layers also occur in close association with river flood deposits associated with an increasing sediment discharge (Ichaso & Dalrymple, 2009). This facies is interpreted as IHS deposits formed by lateral migration of point bars, most probably, in a tide-influenced setting.

4.1.10 | Lithofacies HMi: Inclined-bedded heterolithic mudstone

This lithofacies comprises interbedded very fine-grained sandstones, siltstones and mudstones, with sand:mud ratios of between 10:90 and 40:60, characterised by high-angle inclined lamination (Figure 3J). Commonly, lithofacies HMi shows syn-depositional microfaults and slumped layers (Figure 3J). This facies is very often lenticular bedded. Rarely, mud clasts are present in this facies (Figure 3J). Bioturbation is rare to low characterised by occasional *Arenicolites* and *Taenidium* traces (Figure 4D,E) and also indeterminate horizontal burrows (BI 1–2).

The inclined sand and mud layers were most probably produced by seasonal fluvial floods, within a tide-influenced setting. When fluvial processes were relatively weaker, tidal action predominated, leading to the deposition of muddy IHS characterised by lenticular bedding and muddy/silty interlayers. Soft-sediment deformation reflects loading and rapid deposition on water-logged sediment on an inclined surface (Allen, 1977). This lithofacies is interpreted as IHS deposits formed by lateral migration of point bars.

4.1.11 | Lithofacies HM: Heterolithic mudstone

The mud-dominated heterolithic facies (Lithofacies HM) is characterised by mixed sand–mud heterolithics, with sand:mud ratios varying between 10:90 and 40:60 (Figure 3K). This facies shows dominantly wavy and commonly lenticular bedding, together with current, wave and/or combined-flow ripples. Soft-sediment deformation and syn-depositional microfaults are also present in this facies (Figure 3K). Bioturbation is sparse to low with scattered *Arenicolites*, *Thalassinoides* (Figure 4F) and indeterminate horizontal burrows (BI 0–2).

The sand beds and lenses represent energetic pulses in a broadly low-energy setting where background sedimentation was dominated by mud settling out of suspension (Reineck & Wunderlich, 1968; Shanley et al., 1992). During the higher energy pulses, sand was moved by both unidirectional and oscillatory (wave-generated) flows (Gil-Ortiz et al., 2019). The presence of a spectrum of small-scale combined-flow structures suggests flow variation during deposition (Dumas et al., 2005; Ichaso & Dalrymple, 2014), from oscillatory to unidirectional currents reflecting the superimposition of river flood or tidal currents on wave action.

20554877, 0, Downloaded from https://onlinelibrary.wiley.com/doi/10.1002/dep2.282 by Readcube (Labtiva Inc.), Wiley Online Library on [14/05/2024]. See the Terms and Conditions (https://onlinelibrary.wiley.com/terms-and-conditions) on Wiley Online Library for rules of use; OA articles are governed by the applicable Creative Commons License

4.1.12 | Lithofacies Fm: Massive to laminated mudstone

Lithofacies Fm consists principally of metre-scale bedsets of claystones, muddy siltstones or siltstones. This lithofacies is composed of red to dark grey, massive and/or thin-laminated mudstones with abundant pedogenic features such as rhizoliths, mottling, nodules, cutans, slickensides, indeterminate trace fossils and *Taenidium burrows* (Figure 3L). Horizons marked by desiccation cracks and both coal and dark carbonaceous shales, characterised by horizontal lamination, are also present. This lithofacies is also characterised by low to intense bioturbation (BI 2–5), although, in these muddy, dark red-coloured sediments, bioturbation is commonly difficult to distinguish with confidence. (Figure 3L).

Mudstone deposits with abundant bioturbation, palaeosols and desiccation cracks levels imply low energies and subaerial emergence. This lithofacies is interpreted as the deposits of a floodplain characterised by widespread palaeosol development and/or deposition from suspension in a floodplain swamp environment.

4.2 | Point bar geobody 1: Fluvial point bar

4.2.1 | Description

The geobody in Outcrop 1 occurs as an asymmetrical, sigmoidal-shaped body, up to 3.6 m thick and with a lateral extension of up to 40 m (perpendicular to flow). This geobody is bounded by a horizontal and scoured base, while the top is horizontal and undulatory (Figure 5A,B). This geobody is recognised in outcrop by the occurrence of several inclined master bedding surfaces, showing an upward increase in dip angle (Figure 5C).

This example is characterised by a fining-upward facies succession passing from mudstone rip-up clast conglomerate to very fine-grained sandstones, with relatively high proportions of cross-bedded sandstone (over 35%) and low heterogeneity (less 9% of fines; Figure 6). Internally, these deposits comprise sets of trough cross-bedded sandstone (Lithofacies St) and current ripple cross-laminated (Sr) sandstone towards the top of the facies sequence (Figure 7). Commonly, conglomerate lag deposits (Gm) are located at the base of these sets. Locally, mud drapes also occur between the inclined master surfaces. These elements pinch-out laterally, reducing the thickness of the body to only 1.5 m (red; Figure 5C). In addition, conglomerate lag deposits (Gm) and mud drapes laterally disappear together with a considerable reduction of trough cross-bedded (St) sandstones (less 2%) and current ripple cross-laminated (Sr) sandstone (up to 90%), while parallel-laminated (Sh) sandstone (up to 22%) become notably more common (Figures 6 and 7D,E). Rare *Taenidium* and *Arenicolites* traces are occasionally identified although most bioturbation is restricted to rhyzoliths in the upper muddy section of the point bar.

Towards the top of the geobody, small lenticular bodies are recognised up to 0.8 m thick and with a lateral extension of up to 3 m. These bodies are characterised by parallel-laminated (Sh) and current ripple cross-laminated (Sr) sandstone or, less commonly, small-scale trough cross-bedded (St) sandstones (Figure 5D).

The GR of this geobody is characterised by a cleaning-upward (funnel shape) profile at the base, and a dirtying-upward (bell shape) towards the top (Figure 7A), with API values ranging from 35 to 182. Dip tadpole analysis, with a total of 32 measurements, shows principally unidirectional azimuths and low to high dip angles of lateral accretion surfaces. These measurements show predominantly northeast dipping lateral accretion surfaces, with a mean azimuth of N14E, ranging from N0E to N359E (Figure 7A).

4.2.2 | Interpretation

These asymmetrical sigmoidal geometries, observed in outcrop, together with the characteristic occurrence of several inclined surfaces perpendicular to the palaeocurrent and the fining-upward succession suggest point bar deposits. The inclined surfaces with increasing dip angle are thus interpreted as lateral accretion surfaces, forming a point bar element (sensu Bridge, 1993). The vertical succession of facies reflects lower velocity flows developing progressively through the filling of the channel (Visher, 1965). The presence of current ripples flowing upslope along these accretion surfaces (i.e. perpendicular to the palaeoflow) is interpreted as the result of the helicoidal flow developed in the meander bend (Viseras et al., 2018). The occurrence of mud drapes between the lateral accretion surfaces represents deposition during a waning flood stage (Thomas et al., 1987; Viseras et al., 2018). The small lenticular bodies at the top of the point bar are interpreted as chute channels, on the basis of a fining-upward trend, geobody dimensions, geometry and context within the point bar element. The horizontal-laminated (Sh) and current-rippled (Sr) sandstones represent deposition during higher flood stages (Nemec & Postma, 1993; Miall, 1996; Ghinassi, 2011). During this phase, the water overtops the point bar, scouring the chute channels (Briant, 1983; Ghinassi, 2011). The basal coarsening-upward (funnel shape) interval in the GR log would correspond to the presence of mudstone rip-up clasts (Selley, 2004; Viseras et al., 2018). The presence of scarce horizontal-feeding *Arenicolites* and *Taenidium*

20554877, 0, Downloaded from https://onlinelibrary.wiley.com/doi/10.1002/dep2.282 by Readcube (Labtiva Inc.), Wiley Online Library on [14/05/2024]. See the Terms and Conditions (https://onlinelibrary.wiley.com/terms-and-conditions) on Wiley Online Library for rules of use; OA articles are governed by the applicable Creative Commons License

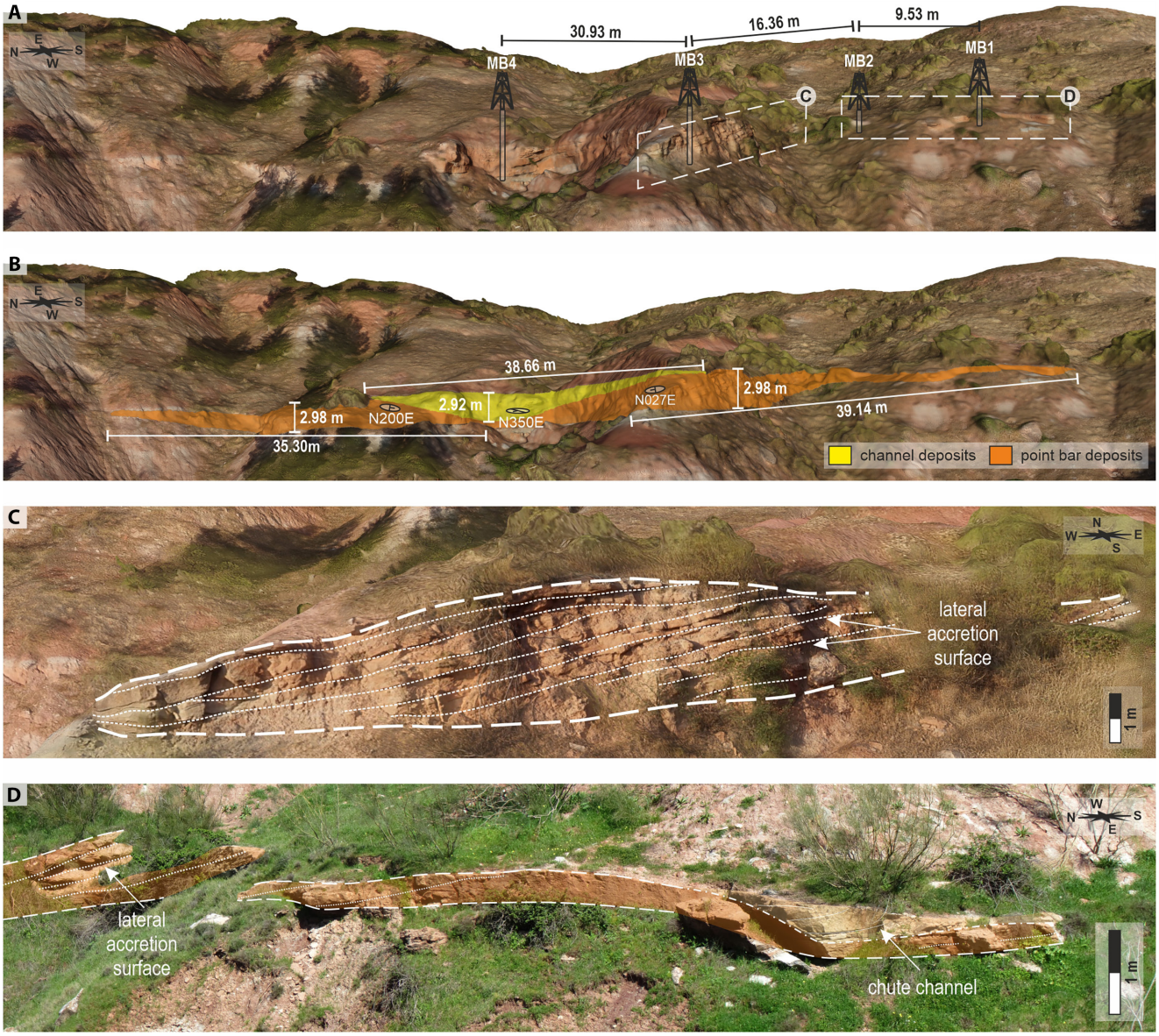

FIGURE 5 Outcrop interpretation of a Fluvial-dominated point bar. (A) Digital outcrop model of Outcrop 1 showing well locations. (B) Interpreted digital outcrop model of Outcrop 1 showing width, thickness and orientation measurements for both channel and point bar deposits. (C, D) Interpreted close-up views of fluvial-dominated point bar deposits showing chute channel deposits.

burrow assemblages are interpreted as the *Mermia-Scoyenia* Ichnofacies, characteristic of freshwater deposits (Diéz-Canseco et al., 2015). The absence of any other marine indicators in this point bar geobody might indicate deposition in a fully fluvial setting.

4.3 | Point bar geobody 2: Tide-influenced point bar

4.3.1 | Description

Geobody 2 occurs in outcrop as an asymmetrical, sigmoidal-shaped body, up to 3.7 m thick with a lateral extension of up to 62 m (apparent width, perpendicular to flow) in outcrop. However, in wells, its thickness can be up to 8 m. This geobody is bounded by a scoured base, while the top is horizontal and undulatory (Figure 8A,B). Several inclined master bedding surfaces are recognised in outcrop (Figure 8C).

This example is characterised by a fining-upward facies succession passing from mudstone rip-up clast conglomerate through very fine-grained sandstones into heterolithic mudstones (Figure 9). Common conglomerate lag deposits (over 19%), cross-bedded sandstone (over 29%) and medium heterogeneity (over 13% of heterolithic sandstones) are observed in this geobody (Figure 10). Internally, this geobody is composed of several fining-upward sets, each characterised by basal reactivation surfaces and rip-up

20554877, 0, Downloaded from https://onlinelibrary.wiley.com/doi/10.1002/dep2.282 by Readcube (Labtiva Inc.), Wiley Online Library on [14/05/2024]. See the Terms and Conditions (https://onlinelibrary.wiley.com/terms-and-conditions) on Wiley Online Library for rules of use; OA articles are governed by the applicable Creative Commons License

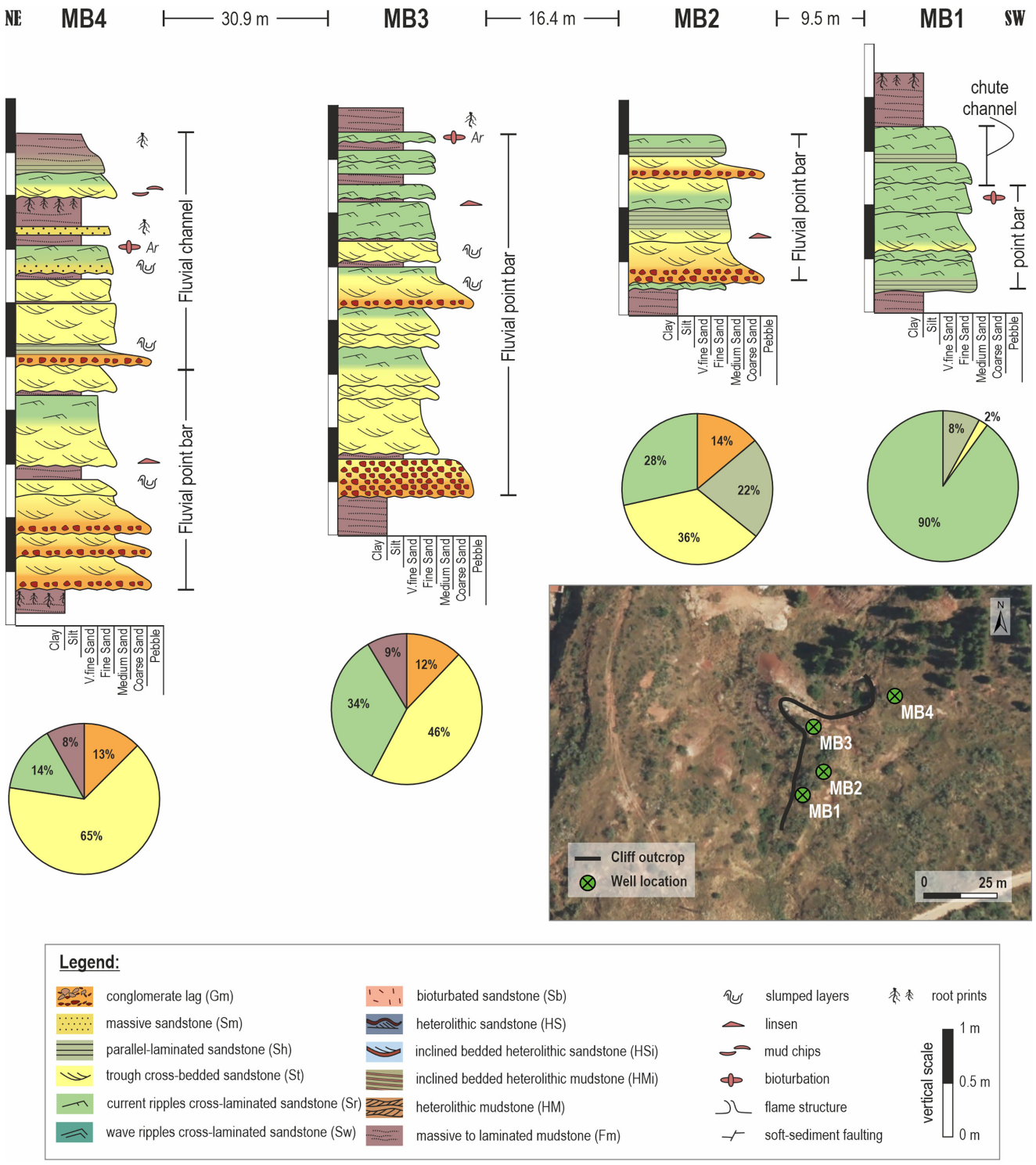

FIGURE 6 Well cross-section containing four wells (MB1-MB4), drilled at Outcrop 1. Sedimentological logs and lithofacies proportions from core description are shown for each well. A digital orthophotography map showing the outcrop-cliff and well locations is also displayed.

mud clasts (Gm), trough cross-bedding (St) very-fine sandstones, inclined-bedded heterolithic (HSi) sandstones and inclined-bedded heterolithic (HMi) mudstones towards the top, respectively (Figure 11). Commonly, soft-sediment deformation (convolute lamination) and pebble-size mudclast foresets are observed in sandstone beds within the inclined-bedded heterolithic (HMi) mudstone facies. Locally, mud drapes also occur between the inclined master surfaces. Laterally, an increase in parallel-laminated (Sh) sandstone and current ripple

20554877, 0, Downloaded from https://onlinelibrary.wiley.com/doi/10.1002/dep2.282 by Readcube (Labtiva Inc.), Wiley Online Library on [14/05/2024]. See the Terms and Conditions (https://onlinelibrary.wiley.com/terms-and-conditions) on Wiley Online Library for rules of use; OA articles are governed by the applicable Creative Commons License

FIGURE 7 Summary of subsurface data for the fluvial-dominated point bar example (Point bar geobody 1). (A) Gamma ray and sedimentological log from Well MB3. Azimuth rose diagram of lateral accretion surfaces is also shown. (B) Slabbed core views from Well MB3. (C–E) Slabbed core views from Wells MB4, MB2 and MB1, respectively. See Figure 6 for the locations of the wells.

cross-laminated (Sr) sandstone is observed (Figures 9 and 11). Rare, flame structures are also present in lithofacies Sh. In addition, thin sets of bioturbated (Sb) sandstones and wave ripple cross-laminated (Sw) sandstones appear towards the top of this geobody. Locally, towards the top of the geobody, lenticular bodies are recognised (Figure 8D),

20554877, 0, Downloaded from https://onlinelibrary.wiley.com/doi/10.1002/dep2.282 by Readcube (Labtiva Inc.), Wiley Online Library on [14/05/2024]. See the Terms and Conditions (https://onlinelibrary.wiley.com/terms-and-conditions) on Wiley Online Library for rules of use; OA articles are governed by the applicable Creative Commons License

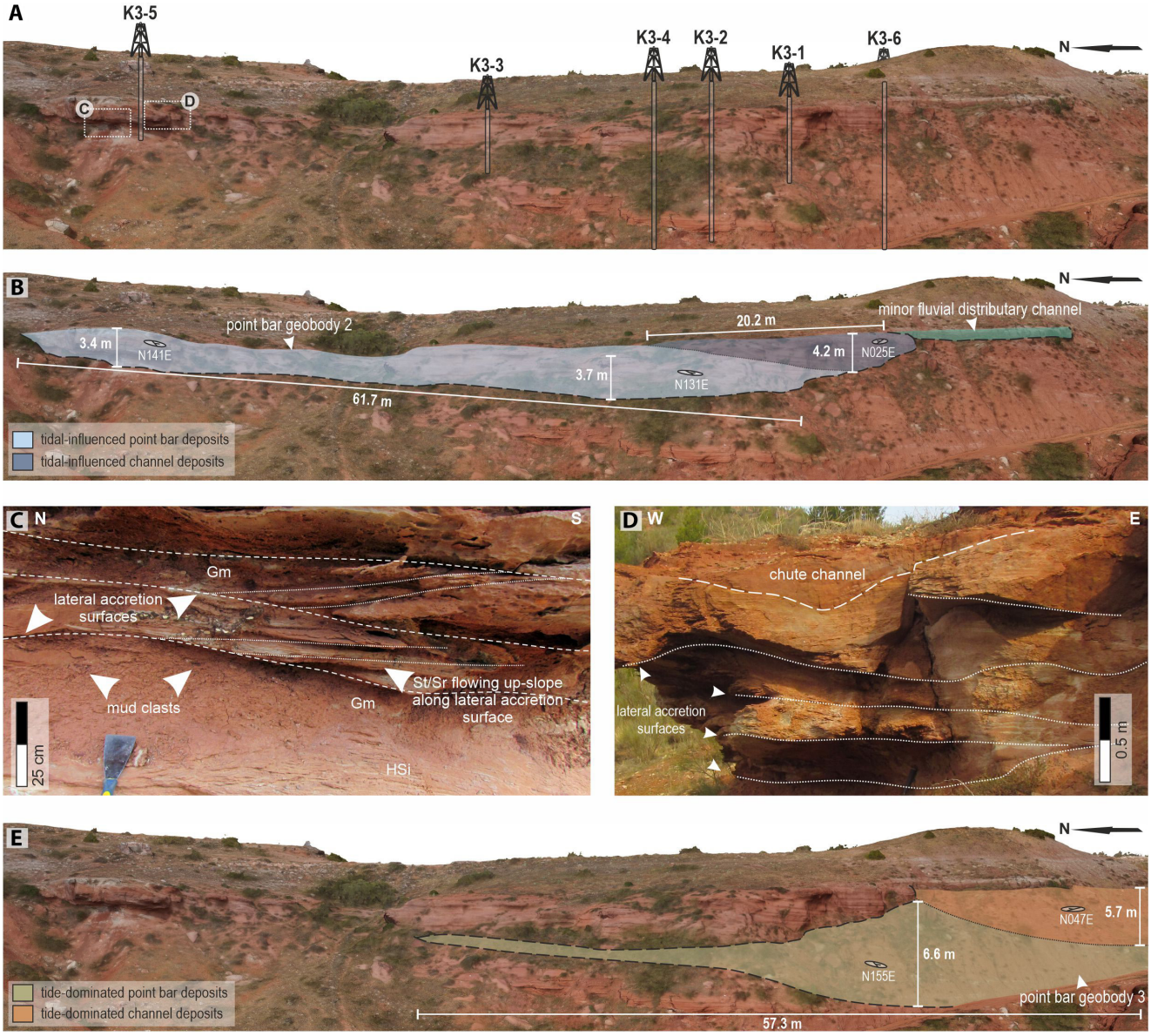

FIGURE 8 Outcrop interpretation of both tide-influenced and tide-dominated point bars. (A) Digital outcrop model of Outcrop 2 showing well locations. (B) Interpreted digital outcrop model of Point bar geobody 2 showing width, thickness and orientation measurements for both channel and point bar deposits. (C) Interpreted close-up view of tide-influenced point bar deposits, showing lateral accretion surfaces and lithofacies in outcrop. (D) Interpreted close-up view of tide-influenced point bar deposits showing lateral accretion surfaces and chute channel deposits. (E) Interpreted digital outcrop model of Point bar geobody 3 showing width, thickness and orientation measurements for both channel and point bar deposits.

up to 0.5 m thick and with a lateral extension of up to 2 m. These bodies are predominantly characterised by trough cross-bedded (St) sandstones and current ripple cross-laminated (Sr) sandstone.

The GR response of this geobody is characterised by values ranging from 63 to 188 API, with a mean of 119 API and a bell-shape profile followed by a cylindrical shape (Figure 11A,B). Dip tadpole analysis, based on a total of 34 measurements, principally shows unidirectional azimuths and low to high dip angles. The predominant azimuths of lateral accretion surfaces are towards the south-east, with a mean azimuth of N140E, ranging from N132E to N146E based on an average of measurements of Wells K3-2, K3-3, K3-4 and K3-5.

4.3.2 | Interpretation

As in the case of point bar geobody 1, this geobody is also interpreted as point bar element (sensu Bridge, 1993). However, the significant proportion of heterolithic sandstones, especially towards the base of the geobody, coupled

20554877, 0, Downloaded from https://onlinelibrary.wiley.com/doi/10.1002/dep2.282 by Readcube (Labtiva Inc.), Wiley Online Library on [14/05/2024]. See the Terms and Conditions (https://onlinelibrary.wiley.com/terms-and-conditions) on Wiley Online Library for rules of use; OA articles are governed by the applicable Creative Commons License

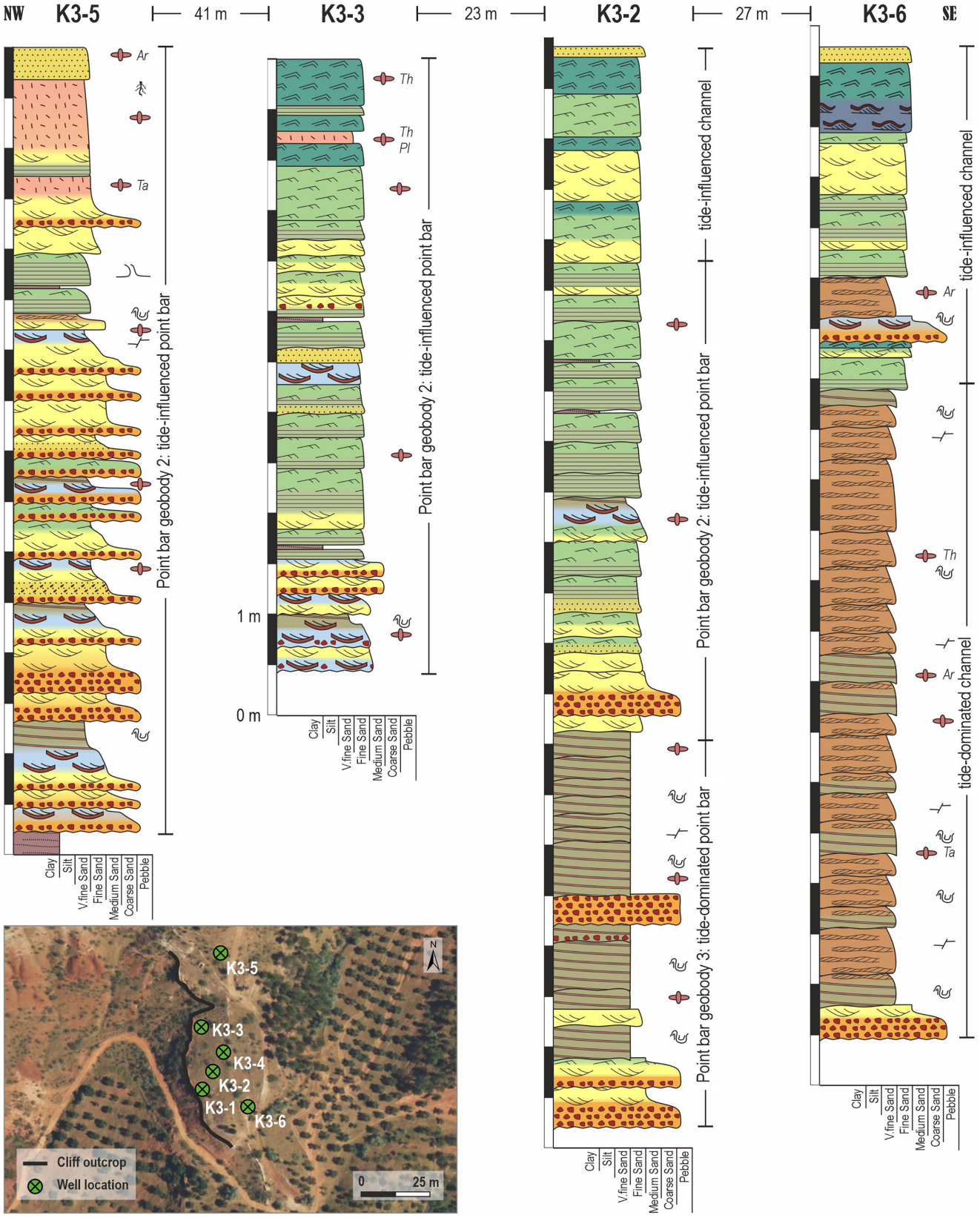

FIGURE 9 Well cross-section containing four wells (K3-2, K3-3, K3-5 and K3-6), drilled at Outcrop 2. Sedimentological logs from core description are shown for each well. A digital orthophotography map showing both outcrop-cliff and well locations is also displayed. See Figure 5 for legend. Key to ichnofossils types: Ar, *Arenicolites*; Pl, *Planolites*; Ta, *Taenidium*; Th, *Thalassinoides*.

20554877, 0, Downloaded from https://onlinelibrary.wiley.com/doi/10.1002/dep2.282 by Readcube (Labtiva Inc.), Wiley Online Library on [14/05/2024]. See the Terms and Conditions (https://onlinelibrary.wiley.com/terms-and-conditions) on Wiley Online Library for rules of use; OA articles are governed by the applicable Creative Commons License

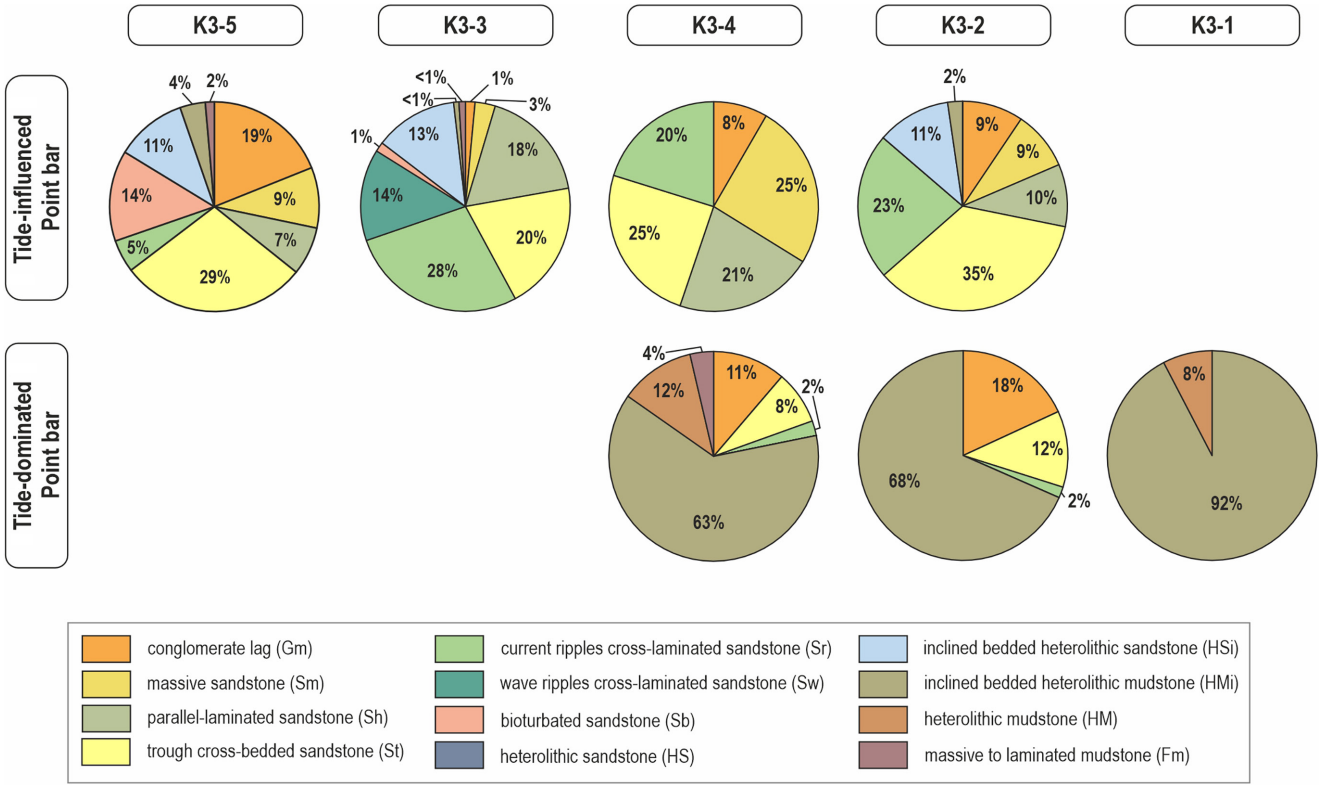

FIGURE 10 Lithofacies proportions derived from the core description of each well drilled in Outcrop 2 divided into tide-influenced point bar (Point bar geobody 2) and tide-dominated point bar (Point bar geobody 3).

with the presence of paired sandstone and mudstones, indicates that tidal currents played an important role in its deposition. Point bar geobody 2 is accordingly interpreted as tide-influenced, a conclusion also supported by a *Mermia-Scoyenia* and *Cruziana* Ichnofacies in some sections, with scattered *Arenicolites*, *Planolites*, *Taenidum*, *Thalassinoides* and indeterminate horizontal deposit-feeding burrows, which place the depositional environment of this point bar in a fluvial–tidal transition zone. As with the fluvial point bar (geobody 1), helicoidal flow is indicated by upslope flowing ripples. The mud drapes intercalated with sandstones and IHS are interpreted as the record of frequent oscillations of energy associated with tidal currents. The small lenticular geobodies located towards the top of the point bar are interpreted as chute channels.

4.4 | Point bar geobody 3: Tide-dominated point bar

4.4.1 | Description

Geobody 3 occurs as packages up to 6.6 m thick and with lateral extensions of up to 52 m (apparent width, perpendicular to flow) in outcrop. This geobody is bounded by both an erosive base and top, truncated by point bar geobody 2. IHS is recognised in outcrop (Figure 8E).

This geobody is characterised by a complete spectrum of heterolithic structures (flaser, wavy and lenticular bedding), with low proportions of cross-bedded sandstone (<14%) and high heterogeneity (over 68% of heterolithic mudstones; Figure 10). Inclined-bedded heterolithic (HMi) mudstones are the dominant lithofacies in this point bar geobody (Figure 12). Dewatered, deformed layers are also observed. In addition, this geobody is also characterised by a basal conglomerate lag (Gm) and several superimposed sets characterised by reactivation surfaces, rip-up mud clasts, trough cross-bedded (St) fine sandstones and fine to very fine sandstones with current ripple cross-lamination (Sr; Figure 12).

In the GR log, geobody 3 is characterised by values ranging from 85 to 202 API, a mean value of 142 API and a cylindrical shape (Figure 12B). Dip tadpole analysis, based on a total of 31 measurements, shows principally unidirectional azimuths and low to high dip angles associated with lateral accretion surfaces. The predominant azimuths are towards the south-east, with a mean azimuth of N155E, ranging from N138E to N168E based on an average of measurements from Wells K3-1, K3-2 and K3-4.

2055-4877, 0, Downloaded from https://onlinelibrary.wiley.com/doi/10.1002/dep2.282 by Readcube (Labtiva Inc.), Wiley Online Library on [14/05/2024]. See the Terms and Conditions (https://onlinelibrary.wiley.com/terms-and-conditions) on Wiley Online Library for rules of use; OA articles are governed by the applicable Creative Commons License

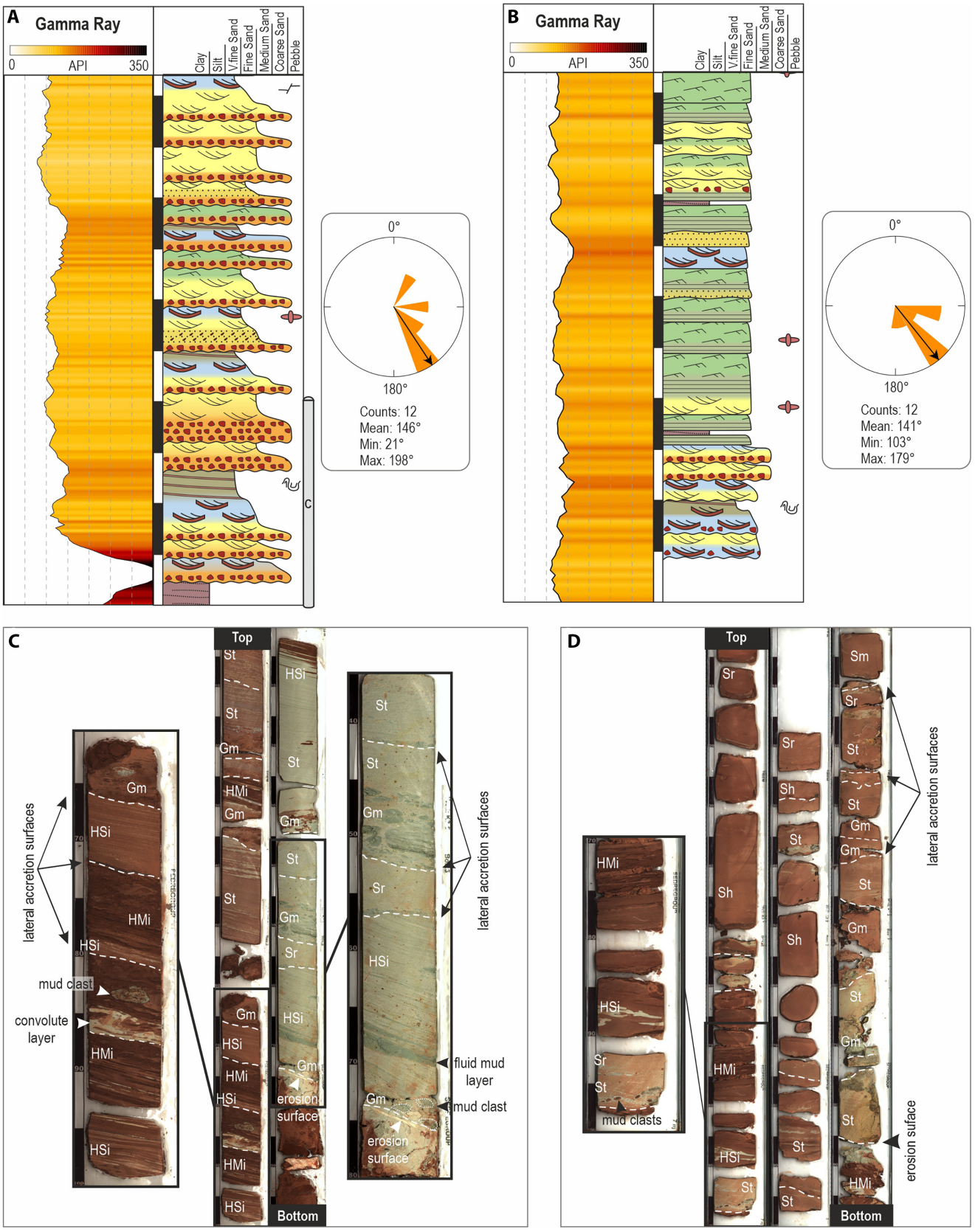

FIGURE 11 Examples of subsurface data from the tide-influenced point bar (Point bar geobody 2). (A) Gamma ray log, sedimentological log and azimuth rose diagram of lateral accretion surfaces from Well K3-5. (B) Gamma ray log, sedimentological log and palaeocurrent rose diagram from Well K3-3. (C, D) Examples of slabbed core from Wells K3-5 and K3-1, respectively. See Figure 9 for the locations of the wells.

20554877, 0, Downloaded from https://onlinelibrary.wiley.com/doi/10.1002/dep2.282 by Readcube (Labtiva Inc.), Wiley Online Library on [14/05/2024]. See the Terms and Conditions (https://onlinelibrary.wiley.com/terms-and-conditions) on Wiley Online Library for rules of use; OA articles are governed by the applicable Creative Commons License

4.4.2 | Interpretation

This geobody is interpreted as a point bar element (sensu Bridge, 1993) as suggested by the presence of IHS and the palaeocurrents (Thomas et al., 1987; Shanley et al., 1992; Dalrymple & Choi, 2007). The basal lag is interpreted as deposited under high energy conditions along the thalweg of tidal or fluvio-tidal channels (Dalrymple & Choi, 2007). Above this, the lithofacies comprising this geobody, mainly characterised by inclined-bedded heterolithic (HMi) mudstones, suggests that the sediment accumulated under fluctuating energy conditions, which may be due to a marine influence. The presence of interbedded sandstone and mudstone shows a subtle rhythmicity, providing evidence for a tidal influence, together with a low-diversity mixed *Mermia-Scoyenia* and *Cruziana* Ichnofacies with scattered *Arenicolites*, *Taenidum*, *Thalassinoides* and indeterminate horizontal deposit-feeding burrows, which support the proximity to a marginal to shallow marine setting. Geobody 3 is interpreted as having accumulated within the point bars of a meandering, tide-dominated channel.

5 | DISCUSSION: TIDAL VERSUS FLUVIAL POINT BAR

The hydrodynamics and sedimentology of both fully fluvial and marine environments have been extensively studied, as have the interaction between tides and rivers in the fluvial–tidal transition zone (Allen, 1991; Cuevas Gozalo & De Boer, 1991; Dalrymple & Choi, 2007; Fischbein et al., 2009; Ghosh et al., 2005; Jablonski & Dalrymple, 2016; La Croix & Dashtgard, 2014; Martinius & Gowland, 2011; Martinius & Van den Berg, 2011; Sisulak & Dashtgard, 2012; Van den Berg et al., 2007).

Key aspects differentiating fluvial point bars from tide-influenced or tide-dominated point bars discussed in this work include frequency and thickness of mud layers, grain-size distribution, cyclicity of bedding and ichnofacies (Table 2). The abundance of these sedimentological features mostly depends on the proximity of coastal high-sinuosity systems to the sea and consequently, the relative position of the river meanders in the fluvial–tidal transition zone, which in marginal marine settings is defined as a transitional zone characterised by a combination of fluvial and tidal processes (Figure 13A). The inner boundary of this transition zone is located at the maximum landward limit of tidal influence, whereas the outer boundary is located at the maximum seaward limit of fluvial-dominated dynamics (Dalrymple & Choi, 2007; Figure 13A). The seaward decrease in the intensity of river flow and the seaward increase in the intensity of tidal currents become the key to understanding the different sedimentary processes operating within the fluvial–tidal transition zone.

The frequency and thickness of mud layers constitute a critical point in the sedimentological analysis. A key aspect regarding this issue is to properly differentiate whether the presence and amount of mud is exclusively controlled by the relative position of point bars in a fluvial or fluvial–tidal zone with respect to the shoreline (Figure 13A), or if it is due to energy fluctuations related to unidirectional flow discharges within a meander belt. The former case may be characterised in terms of the difference between regular or extensional point bars and translating or counter point bars (Smith et al., 2009; Hubbard et al., 2011; Durkin et al., 2020).

Whereas a regular sandy point bar may present an increase in shale content, depending on its relative position with respect to upstream (less mud content) or downstream location (more mud content), a counter or translating point bar may present a characteristic heterolithic to mud-prone fabric, even in a purely fluvial setting. A quantitative analysis of the mud layers, lateral evolution of sedimentary structures and ichnofacies interpretation may thus become crucial in distinguishing between these two cases. A plan view of these deposits could also provide insight into the convex or concave-bank shape of these point bars. Regular point bars are typically deposited under a convex scroll pattern, whereas translating point bars normally present a characteristic concave scroll pattern, although in this case, the exposure of the studied deposits is very limited from this perspective.

As demonstrated by this study, fluvial point bars (point bar geobody 1) normally present sand-prone facies with a characteristic fining-upward succession and low to very low mud content, almost always restricted to the upper part of the geobody, mostly representing the abandonment of the active channel and subsequent frequent colonisation by land flora (Figure 13B). Fluvial deposits of this type may act as excellent reservoirs in the subsurface and have been successfully tested as potential reservoirs for CO_2 injection and storage (Issautier et al., 2014, 2016; Gershenzon et al., 2015, 2017; Soltanian, et al., 2019; Sun et al., 2023).

Downstream, the tidal influence increases as the continental fluvial plain reaches the fluvial–tidal transition zone. This is so, as long as both the coastal plain gradient is sufficiently low and provided there is a reasonable and effective tidal range, allowing tides to travel upstream and interact with fluvial processes along the river course. This is especially highlighted in point bar geobody 2, where heterolithic layers are seen to increase in volume by more than 25% in some well sections and also to show

20554877, 0, Downloaded from https://onlinelibrary.wiley.com/doi/10.1002/dep2.282 by Readcube (Labtiva Inc.), Wiley Online Library on [14/05/2024]. See the Terms and Conditions (https://onlinelibrary.wiley.com/terms-and-conditions) on Wiley Online Library for rules of use; OA articles are governed by the applicable Creative Commons License

FIGURE 12 Subsurface data from the tide-dominated point bar example (Point bar geobody 3). (A) Gamma ray log, sedimentological log and azimuth rose diagram of lateral accretion surfaces from Well K3-4. (B) Gamma ray log, sedimentological log and palaeocurrent rose diagram from Well K3-2. (C–E) Slabbed core views from Wells K3-4, K3-2 and K3-1, respectively. See Figure 9 for the locations of the wells.

significantly thicker mudstone drapes over primary sedimentary structures such as trough cross-bedding and current ripple cross-lamination.

The presence of mostly inclined heterolithic sandstones, but also heterolithic mudstones, between major lateral accretion surfaces and the frequency of thin centimetre to decimetre-thick fining-upward sandstone successions also highlights the role of energy fluctuations mostly associated with tidal interaction in a fluvial–tidal transition zone (Allen, 1991; Cuevas Gozalo & De Boer, 1991; Ghosh et al., 2005; Makaske & Weerts, 2005; Dalrymple & Choi, 2007; Van den Berg et al., 2007;

20554877, 0, Downloaded from https://onlinelibrary.wiley.com/doi/10.1002/dep2.282 by Readcube (Labtiva Inc.), Wiley Online Library on [14/05/2024]. See the Terms and Conditions (https://onlinelibrary.wiley.com/terms-and-conditions) on Wiley Online Library for rules of use; OA articles are governed by the applicable Creative Commons License

TABLE 2 Comparative table of the key features differentiating point bars according to their sub-environment identified in this study.

Point bar sub-environment	Grain-size distribution	Frequency and thickness of mud layers	Repetition of sequences/cyclicity	Ichnofacies assemblage and other bioturbation traces
Fluvial	Fining-upward sandy sequences Average sand:mud ratio 90:10	Thin commonly bioturbated cm-scale mud layers restricted towards the upper part of the sequences	Cyclicity not observed	Mermia-Scoyenia ichnofacies. Common palaeosols
Tide-influenced	Vertically stacked cm-to dm-fining-upward sandy to sandy heterolithic sequences Average sand:mud ratio 75:25	Mud drapes on primary sedimentary structures and sandy heterolithics (IHS)	Certain repetition of cm-sandy heterolithic sequences	Mixed *Mermia-Scoyenia* and *Cruziana* ichnofacies
Tide-dominated	Aggradational cm-scale silty to muddy heterolithic sequences Average sand:mud ratio 20:80	Mud drapes on primary sedimentary structures and muddy heterolithics (IHS)	Certain repetition of cm-muddy heterolithic sequences	Mixed *Mermia-Scoyenia* and *Cruziana* ichnofacies

Fischbein et al., 2009; Martinius & Gowland, 2011; Martinius & Van den Berg, 2011; Fustic et al., 2012; Musial et al., 2012; Sisulak & Dashtgard, 2012; La Croix & Dashtgard, 2014; Carling et al., 2015; Dashtgard & La Croix, 2015; Díez-Canseco et al., 2015; Keevil et al., 2015; Jablonski & Dalrymple, 2016).

The vertical evolution of sedimentary structures also shows a waning trend between sequences bounded by erosive surfaces, apparently with a certain repetition under energy fluctuations. The fining-upward grain-size distribution, presence of IHS and mud drapes is interpreted in terms of deposition of tide-influenced point bars (Figure 13C).

An alternative explanation for the increase of mud content and heterolithic fabric in these deposits might be on the basis of a different depositional pattern, perhaps due to the presence of a high resistive layer on the valley margin offering resistance to downstream flow, thereby initiating a translating migration of the point bar and deposition of a counter point bar (Page & Nanson, 1982; Nanson & Page, 1983; Smith et al., 2009; Hubbard et al., 2011; Ghinassi et al., 2016, 2018; Durkin et al., 2020; Fietz et al., 2021).

However, the generally fine to very fine-grained size, the moderate to relatively good sorting of sandstones, associated with not only a long source to sink distance but also an effective mechanism of sediment washing (such as waves or tides; Gil-Ortiz et al., 2019, 2022) and the limited, but characteristic, *Mermia-Scoyenia* and *Cruziana* Ichnofacies present in this geobody all suggest the initial interpretation of a tide-influenced point bar that is preferred here.

The point bar geobody 3, shows a lower section mostly comprising inclined heterolithic mudstone layers and heterolithic mudstones interpreted as IHS associated with deposition of point bars in a protected low-energy setting. In this case, there is a more than 70% increase in muddy lithofacies content relative to the tide-influenced point bar. The sand to mud ratio is around 20:80, highlighting a major decrease in the energy of the system, showing a very homogeneous grain-size distribution. Furthermore, there is also a certain repetition of centimetre-thick, inclined heterolithic mudstones and heterolithic mudstones showing a cylindrical GR profile associated with a gentle fining-upward shaly section, interpreted as tide-dominated point bar and channel deposits in a protected low energy transitional non-marine to shallow marine environment (Figure 13D). A mixed *Mermia-Scoyenia* and *Cruziana* ichnofacies assemblage was also identified supporting the interpretation of a marginal marine setting close to the shoreline.

Once again, an alternative scenario is also possible, considering the probable occurrence of counter point

20554877, 0, Downloaded from https://onlinelibrary.wiley.com/doi/10.1002/dep2.282 by Readcube (Labtiva Inc.), Wiley Online Library on [14/05/2024]. See the Terms and Conditions (https://onlinelibrary.wiley.com/terms-and-conditions) on Wiley Online Library for rules of use; OA articles are governed by the applicable Creative Commons License

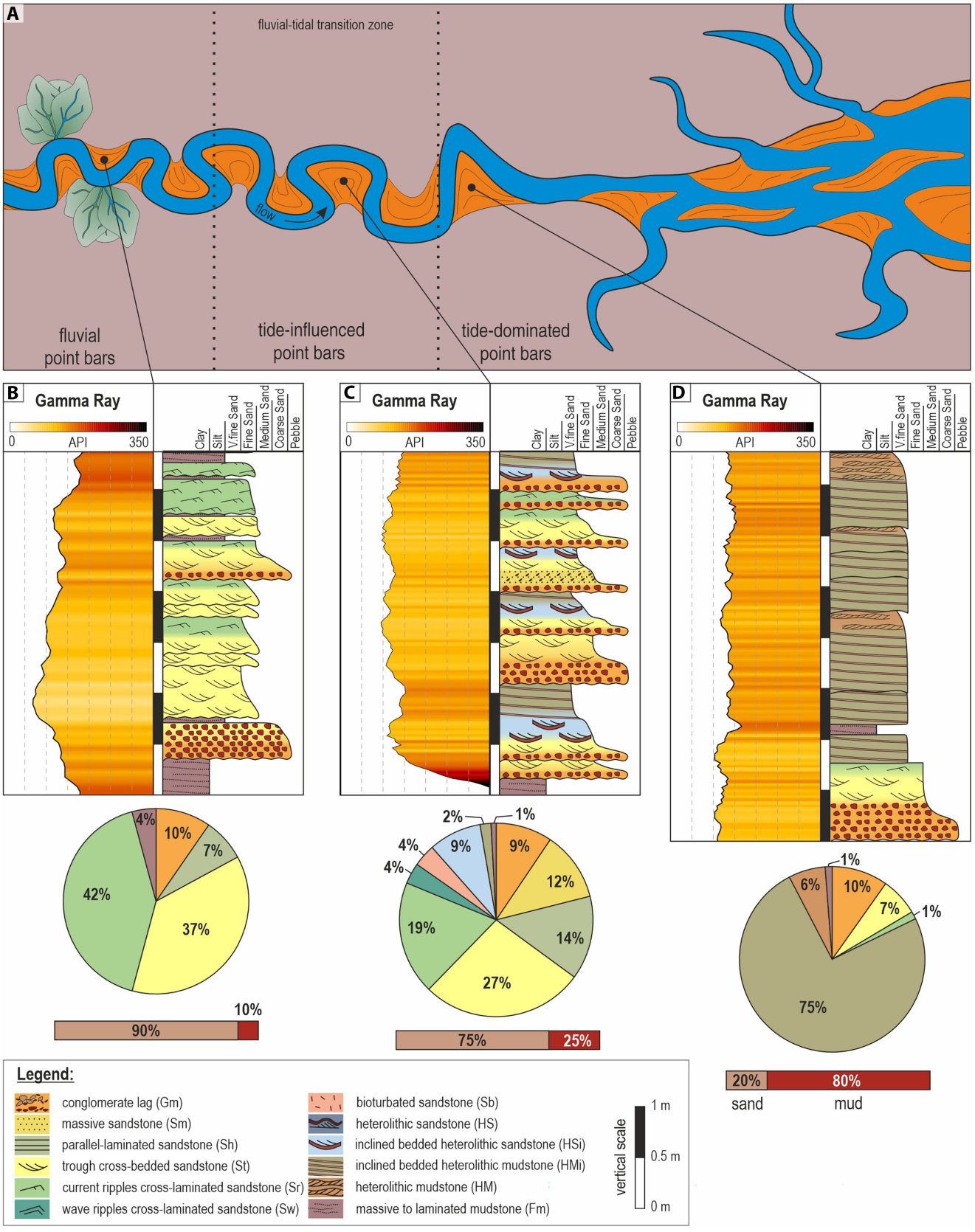

FIGURE 13 (A) Schematic diagram showing the possible spatial zones for the deposition of the different types of point bar. (B, C) Gamma ray logs, sedimentological logs, lithofacies proportions and sand: mud ratio for, respectively, a fluvial-dominated point bar (Point bar geobody 1), a tide-influenced point bar (Point bar geobody 2) and a tide-dominated point bar (Point bar geobody 3).

20554877, 0, Downloaded from https://onlinelibrary.wiley.com/doi/10.1002/dep2.282 by Readcube (Labtiva Inc.), Wiley Online Library on [14/05/2024]. See the Terms and Conditions (https://onlinelibrary.wiley.com/terms-and-conditions) on Wiley Online Library for rules of use; OA articles are governed by the applicable Creative Commons License

bar deposits intercalated in a more proximal domain with fluvial deposits, although the fine-grained to very fine-grained size and good sorting of sandstones, together with the additional ichnofossil data from these deposits, strongly favour a distal fluvial–tidal transition zone as the more probable setting for the deposition of this point bar.

6 | CONCLUSIONS

The TIBEM succession shows an exceptional record of fluvial to tide-dominated high-sinuosity river deposits. The studied section includes three point bar geobodies from two selected outcrops; a point bar in the lower continuous tabular M-S Unit and two other point bars in an upper incised valley infilling H Unit.

This high-resolution sedimentological study, combining outcrop and subsurface data, highlights the complex interaction of depositional processes in channels within the fluvial–marine transition zone. It also emphasises the need to establish key criteria that aid in identifying the position of these channels within the fluvial–marine transition zone, as this has potentially significant implications when assessing these geobodies as reservoirs.

On the basis of grain-size distribution, frequency and thickness of mudstone beds, cyclicity of bedding and ichnofacies, three different point bar types were identified, ranging from a fluvial system to a tide-dominated marginal marine environment. The three types of point bar geobodies studied exhibit similar dimensions, representing identical equivalent potential reservoir volumes. However, the grain-size distribution, clay content and frequency of mud layers, representing potential permeability barriers/baffles they present, will differ significantly between the point bar types.

The fluvial point bar (Point bar geobody 1) is the geobody with the least heterogeneity from the three studied, characterised by fining-upward sandy sequences and a sand:mud ratio of 90:10. The tide-influenced point bar (Point bar geobody 2) exhibits heterogeneous facies at the base, while sandy facies predominate towards the top. This is characterised by vertically stacked decimetre to centimetre-thick fining-upward sandy to sandy heterolithic sequences and a sand:mud ratio of 75:25. In contrast, the tide-dominated point bar (Point bar geobody 3) is characterised by aggradational centimetre-scale, silty to muddy heterolithic sequences and a sand:mud ratio of 20:80, presenting purely sandy facies only at its base. This point bar geobody may represent a potential lateral barrier of some significance when considering it as reservoir in the subsurface.

The presence of mud drapes as potential permeability barriers/baffles is also important, predominant in both the fluvial point bar (Point bar geobody 1) and the tide-influenced point bar (Point bar geobody 2). However, thicker mud layers, as well as the presence of paired sand and mud layers, are typical in the tide-dominated point bar and the tide-influenced point bar (Point bar geobody 3 and 2, respectively), especially towards the base of the latter. In contrast, the fluvial point bar (Point bar geobody 1) shows only thin and rare mud layers, restricted to the top of these deposits, representing the abandonment of the channel and associated with the common occurrence of palaeosol development. The presence of paired sand and mud layers has not been observed in this point bar.

In conclusion, fluvial point bars and tide-influenced point bars would form the best reservoir geobodies in fluvial to fluvial–tidal transition zones, showing the best facies in terms of reservoir quality. However, it is worth noting that the presence of mud drapes may impede internal lateral continuity. Tide-dominated point bars, in contrast, given the greater potential for flow baffles/barriers and notably lower net to gross, should be carefully characterised and identified in the subsurface to properly manage reservoir capacity and fluid flow evolution.

ACKNOWLEDGEMENTS

Grants PID2022-140850OB-C21 and PID2022-140850OB-C22 were funded by MCIN/AEI/10.13039/501100011033 and by 'ERDF A way of making Europe'. The Margarita Salas postdoctoral research contract (MS2022-17), Ministry of Universities of Spain, European Union—NextGenerationEU—and the RNM369 Research Group (PAI) is also acknowledged. The authors also thank REPSOL EXPLORACION and CEPSA E.P for their support. Support from the MCIyU/AEI (Grant RTI2018-097312-A-I00MCNN), MCIN/AEI/10.13039/501100011033 and 'European Union NextGenerationEU/PRTR' (Grant TED2021-130602B-I00), and from the Generalitat de Catalunya (2021SGR00076) is gratefully acknowledged. The authors further thank the two anonymous reviewers and the editors Peter Swart and Valentina M. Rossi for their constructive comments that have significantly improved the content of this paper.

CONFLICT OF INTEREST STATEMENT

The authors declare that they have no known competing financial interests or personal relationships that could have appeared to influence the work reported in this paper.

DATA AVAILABILITY STATEMENT

The data supporting the findings of this study are available upon reasonable request from the corresponding author.

20554877, 0, Downloaded from https://onlinelibrary.wiley.com/doi/10.1002/dep2.282 by Readcube (Labtiva Inc.), Wiley Online Library on [14/05/2024]. See the Terms and Conditions (https://onlinelibrary.wiley.com/terms-and-conditions) on Wiley Online Library for rules of use; OA articles are governed by the applicable Creative Commons License

ORCID

Luis Miguel Yeste https://orcid.org/0000-0002-5349-2673
Marc Gil-Ortiz https://orcid.org/0000-0002-4685-6491

REFERENCES

Al-Khdheeawi, E.A., Vialle, S., Barifcani, A., Sarmadivaleh, M. & Iglauer, S. (2017) Influence of injection well configuration and rock wettability on CO_2 plume behaviour and CO_2 trapping capacity in heterogeneous reservoirs. *Journal of Natural Gas Science and Engineering*, 43, 190–206.

Al-Khdheeawi, E.A., Vialle, S., Barifcani, A., Sarmadivaleh, M. & Iglauer, S. (2018) Enhancement of CO_2 trapping efficiency in heterogeneous reservoirs by water-alternating gas injection. *Greenhouse Gases: Science and Technology*, 8(5), 920–931.

Allen, G.P. (1991) Sedimentary processes and facies in the Gironde estuary: a recent model for macrotidal estuarine systems. In: Smith, D.G., Reinson, G.E., Zaitlin, B.A. & Rahmani, R.A. (Eds.) *Clastic tidal sedimentology*. Calgary: Canadian Society of Petroleum Geologists, Memoir 16, pp. 29–40.

Allen, J.R.L. (1963) The classification of cross-stratified units, with notes on their origin. *Sedimentology*, 2, 93–114.

Allen, lR.L. (1977) The possible mechanics of convolute lamination in graded sand beds. *Journal of the Geological Society*, 134, 19–31.

Ambrose, W.A., Lakshminarasimhan, S., Holtz, M.H., Núñez-López, V., Hovorka, S.D. & Duncan, I. (2008) Geologic factors controlling CO_2 storage capacity and permanence: case studies based on experience with heterogeneity in oil and gas reservoirs applied to CO_2 storage. *Environmental Geology*, 54(8), 1619–1633.

Anderson, J.B., Wallace, D.J., Rodriguez, A.B. & Simms, A.R. (2023) Unprecedented historical erosion of US Gulf Coast: a consequence of accelerated sea-level rise? *Earth's Future*, 11, e2023EF003676. https://doi.org/10.1029/2023EF003676

Arche, A. & López-Gómez, J. (2014) The Carnian Pluvial Event in Western Europe: new data from Iberia and correlation with the Western Neotethys and Eastern North America–NW Africa regions. *Earth Science Reviews*, 128, 196–231.

Ashworth, P.J., Best, J. & Parsons, D. (2015) *Fluvial-tidal sedimentology*. Amsterdam and Oxford and Waltham, MA: Elsevier. *Developments in Sedimentology*, 68, 656.

Blum, M., Carter, A.E., Zayac, T. & Goble, R. (2002) Middle Holocene sea-level and evolution of The Gulf of Mexico Coast (USA). *Journal of Coastal Research*, 36, 65–80. https://doi.org/10.2112/1551-5036-36.sp1.65

Boyd, R., Dalrymple, R. & Zaitlin, B.A. (1992) Classification of clastic coastal depositional environments. *Sedimentary Geology*, 80(3–4), 139–150. https://doi.org/10.1016/0037-0738(92)90037-R

Bradley, G., Redfern, J., Hodgetts, D., George, A.D. & Wach, G.D. (2018) The applicability of modern tidal analogues to pre-vegetation paralic depositional models. *Sedimentology*, 65(6), 2171–2201. https://doi.org/10.1111/sed.12461

Briant, I.D. (1983) Facies sequences associated with some braided river deposits of the Late Pleistocene age from southern Britain. *International Association of Sedimentologists. Special Publication*, 6, 267–275.

Bridge, J.S. (1993) Description and interpretation of fluvial deposits: a critical perspective. *Sedimentology*, 40, 801–810.

Broughton. (2016) Alignment of fluvio-tidal point bars in the middle McMurray Formation: implications for structural architecture of the Lower Cretaceous Athabasca Oil Sands Deposit, northern Alberta. *Canadian Journal of Earth Sciences*, 53, 1–35. https://doi.org/10.1139/cjes-2015-0137

Carling, P., Chateau, C., Leckie, D., Langdon, C., Scaife, R. & Parsons, D. (2015) Sedimentology of a tidal point-bar within the fluvial-tidal transition; River Severn Estuary, UK. In: Ashworth, P., Best, J. & Parsons, D.R. (Eds.) *Fluvial-tidal sedimentology*. Amsterdam and Oxford and Waltham, MA: Elsevier. *Developments in Sedimentology*, 68, 149–189.

Chadwick, R., Zweigel, P., Gregersen, U., Kirby, G., Holloway, S. & Johannessen, P. (2004) Geological reservoir characterization of a CO_2 storage site: the Utsira Sand, Sleipner, northern North Sea. *Energy*, 29, 1371–1381.

Collinson, J.D. & Thompson, D.B. (1989) *Sedimentary structures*, 2nd edition. London: Chapman & Hall, p. 207.

Collinson, J.D., Mountney, N. & Thompson, D. (2006) *Sedimentary structures*. Hertfordshire: Terra Publishing.

Cuevas Gozalo, M. & De Boer, P.L. (1991) Tide-influenced fluvial deposits: examples from Eocene of the southern pyrenees. In: Marzo, M. & Puigdefàbregas, C. (Eds.) *Guidebook to the 4th International Conference on Fluvial Sedimentology*. Barcelona: Publicacions del Servei Geològic de Catalunya, p. 92.

Dalrymple, E.W., Kurcinka, C.E., Jablonski, B.V.J., Ichaso, A.A. & Mackay, D.A. (2015) Deciphering the relative importance of fluvial and tidal processes in the fluvial–marine transition. In: Ashworth, P., Best, J. & Parsons, D.R. (Eds.) *Fluvial-tidal sedimentology*. Amsterdam and Oxford and Waltham, MA: Elsevier. *Developments in Sedimentology*, 68, 1–45.

Dalrymple, R.W., Mackay, D.A., Ichaso, A.A. & Choi, K. (2012) Processes, morphodynamics, and facies of tide-dominated estuaries. In: Davis, R.A., Jr. & Dalrymple, R.W. (Eds.) *Principles of tidal sedimentology*. Dordrecht: Springer, pp. 79–107. https://doi.org/10.1007/978-94-007-0123-6_5

Dalrymple, R.W. & Choi, K. (2007) Morphologic and facies trends through the fluvial–marine transition in tide-dominated depositional systems: a schematic framework for environmental and sequence-stratigraphic interpretation. *Earth-Science Reviews*, 81(3–4), 135–174. https://doi.org/10.1016/j.earscirev.2006.10.002

Dalrymple, R.W., Zaitlin, B.A. & Boyd, R. (1992) Estuarine facies models: conceptual basis and stratigraphic implications. *Journal of Sedimentary Research*, 62(6), 1130–1146. https://doi.org/10.1306/D4267A69-2B26-11D7-8648000102C1865D

Dashtgard, S.E., Gingras, M.K. & MacEachern, J.A. (2009) Tidally modulated shorefaces. *Journal of Sedimentary Research*, 79, 793–807. https://doi.org/10.2110/jsr.2009.084

Dashtgard, S.E. & La Croix, A.D. (2015) Sedimentological trends across the tidal-fluvial transition, Fraser River, Canada: a review and some broader implications. In: Ashworth, P., Best, J. & Parsons, D.R. (Eds.) *Fluvial-tidal sedimentology*. Amsterdam and Oxford and Waltham, MA: Elsevier. *Developments in Sedimentology*, 68, 111–126.

Davis, R.A. & Dalrymple, R.W. (Eds.). (2012) *Principles of tidal sedimentology*. New York: Springer Verlag, p. 621.

20554877, 0, Downloaded from https://onlinelibrary.wiley.com/doi/10.1002/dep2.282 by Readcube (Labtiva Inc.), Wiley Online Library on [14/05/2024]. See the Terms and Conditions (https://onlinelibrary.wiley.com/terms-and-conditions) on Wiley Online Library for rules of use; OA articles are governed by the applicable Creative Commons License

Desjardins, P.R., Buatois, L.A. & Mángano, M.G. (2012) Tidal flats and subtidal sand bodies. *Developments in Sedimentology*, 64, 529–561. https://doi.org/10.1016/B978-0-444-53813-0.00018-6

Díez-Canseco, D., Buatois, L.A., Mangano, M.G., Rodríguez, W. & Solorzano, E. (2015) The ichnology of the fluvial–tidal transition: interplay of ecologic and evolutionary controls. In: Ashworth, P., Best, J. & Parsons, D.R. (Eds.) *Fluvial-tidal sedimentology*. Amsterdam and Oxford and Waltham, MA: Elsevier. *Developments in Sedimentology*, 68, 283–321.

Dumas, S., Arnott, R.W.C. & Southard, J.B. (2005) Experiments on oscilatory-flow and combined-flow bed forms: implications for interpreting parts of the shallow marine sedimentary record. *Journal of Sedimentary Research*, 75, 501–5134.

Durkin, P.R., Hubbard, S.M., Holbrook, J., Weleschuk, Z., Nesbit, P., Hugenholtz, C., Lyons, T. & Smith, D.G. (2020) Recognizing the product of concave-bank sedimentary processes in fluvial meander-belt strata. *Sedimentology*, 67(6), 2819–2849. https://doi.org/10.1111/sed.12743

Fernández, J. & Dabrio, C. (1985) Fluvial architecture of the Buntsandstein-facies redbeds in the Middle to Upper Triassic (Ldinian–Norian) of the southeastern edge of the Iberian Meseta (southern Spain). In: Mader, D. (Ed.) *Aspects of fluvial sedimentation in the lower Triassic Buntsandstein of Europe*. Berlin, Heidelberg: Springer. *Lecture Notes in Earth Sciences*, 4, 411–435.

Fietz, S.W., Gingras, M.K., MacEachern, J.A., Rinke-Hardekopf, L. & Dashtgard, S.E. (2021) Sedimentology and neoichnology of a muddy translating point bar in the fluviotidal transition, Serpentine River, BC, Canada. *Sedimentary Geology*, 426, 106028. https://doi.org/10.1016/j.sedgeo.2021.106028

Fischbein, S.A., Joeckel, R. & Fielding, C.R. (2009) Fluvial-estuarine reinterpretation of large, isolated sandstone bodies in epicontinental cyclothems, Upper Pennsylvanian, northern Midcontinent, USA, and their significance for understanding late Paleozoic sea-level fluctuations. *Sedimentary Geology*, 216, 15–28.

Fustic, M., Hubbard, S.M., Spencer, R., Smith, D.G., Leckie, D.A., Bennett, B. & Larter, S. (2012) Recognition of down-valley translation in tidally influenced meandering fluvial deposits, Athabasca Oil Sands (Cretaceous), Alberta, Canada. *Marine and Petroleum Geology*, 29, 219–232.

García-García, F., Yeste, L.M., Henares, S. & Viseras, C. (2017) Tides and waves influence variability on the shoreline systems of the heterolithic unit from the Triassic Tabular Cover of the Iberian Meseta. 33rd IAS Meeting of Sedimentology, 10–12 Oct 2017, Toulouse, France.

Gershenzon, N.I., Ritzi, R.W., Dominic, D.F., Soltanian, M., Mehnert, E. & Okwen, R.T. (2015) Influence of small-scale fluvial architecture on CO_2 trapping processes in deep brine reservoirs. *Water Resources Research*, 51, 8240–8256.

Gershenzon, N.I., Ritzi, R.W., Dominic, D.F. & Mehnert, E. (2017) Effective constitutive relations for simulating CO_2 capillary trapping in heterogeneous reservoirs with fluvial sedimentary architecture. *Geomechanics and Geophysics for Geo-Energy and Geo-Resources*, 3, 265–279.

Ghinassi, M. (2011) Chute channels in the Holocene high-sinuosity river deposits of the Firenze plain, Tuscany, Italy. *Sedimentology*, 58, 618–642.

Ghinassi, M., Ielpi, A., Aldinucci, M. & Fustic, M. (2016) Downstream-migrating fluvial point bars in the rock record. *Sedimentary Geology*, 334, 66–96.

Ghinassi, M., D'Alpaos, A., Gasparotto, A., Carniello, L., Brivio, L., Finotello, A., Roner, M., Franceschinis, E., Realdon, N., Howes, N. & Cantelli, A. (2018) Morphodynamic evolution and stratal architecture of translating tidal point bars: inferences from the northern Venice Lagoon (Italy). *Sedimentology*, 65, 1354–1377.

Ghosh, S.K., Chakraborty, C. & Chakraborty, T. (2005) Influence of fluvial-tidal interactions on the nature of cross-stratified packages in a deltaic setting: examples from the Barakar Coal Measure (Permian), Satpura Gondwana Basin, central India. *Geological Journal*, 40, 65–81.

Gil-Ortiz, M., McDougall, N.D., Cabello, P., Marzo, M. & Ramos, E. (2019) Sedimentology of a "nonactualistic" Middle Ordovician tidal-influenced reservoir in the Murzuq Basin (Libya). *AAPG Bulletin*, 103(9), 2219–2246. https://doi.org/10.1306/02151918138

Gil-Ortiz, M., McDougall, N.D., Cabello, P., Marzo, M. & Ramos, E. (2022) Sedimentary architecture of a Middle Ordovician embayment in the Murzuq Basin (Libya). *Marine and Petroleum Geology*, 135, 105339. https://doi.org/10.1016/j.marpetgeo.2021.105339

Gingras, M.K., MacEachern, J.A., Dashtgard, S.E., Ranger, M.J. & Pemberton, S.G. (2016) The significance of trace fossils in the McMurray formation, Alberta, Canada. *Bulletin of Canadian Petroleum Geology*, 64, 233–250.

Glangeaud, L. (1938) Transport et sedimentation dans l'es tuaire et a l'embouchure de la Gironde. Caracteres Petrographiques des Formations Fluviatiles, Saumatres, Littordes, et Nkritiques. *Bulletin de la Société Géologique de France*, 8, 599–630.

Harris, P.T. & Heap, A.D. (2003) Environmental management of clastic coastal depositional environments: inferences from an Australian geomorphic database. *Ocean and Coastal Management*, 46(5), 457–478. https://doi.org/10.1016/S0964-5691(03)00018-8

Harris, P.T., Heap, A.D., Bryce, S.M., Porter-Smith, R., Ryan, D.A. & Heggie, D.T. (2002) Classification of Australian clastic coastal depositional environments based upon a quantitative analysis of wave, tidal, and river power. *Journal of Sedimentary Research*, 72(6), 858–870. https://doi.org/10.1306/040902720858

Hayes, D.A., Ranger, M.J., Timmer, E.R. & Gingras, M.K. (2018) A sedimentological, ichnological, and architectural comparison of estuarine and fluvial outcrops using UAVbased outcrop modelling in the lower Cretaceous McMurray Formation. *Reservoir*, 45, 8–15.

Henares, S., Caracciolo, L., Cultrone, G., Fernández, J. & Viseras, C. (2014) The role of diagenesis and depositional facies on pore system evolution in a Triassic outcrop analogue (SE Spain). *Marine and Petroleum Geology*, 51, 136–151.

Henares, S., Caracciolo, L., Viseras, C., Fernández, J. & Yeste, L.M. (2016) Diagenetic constraints on heterogeneous reservoir quality assessment: a Triassic outcrop analogue of meandering fluvial reservoirs. *AAPG Bulletin*, 100(9), 1377–1398.

Hill, P.R., Meulé, S. & Longuépée, H. (2003) Combined flow processes and sedimentary structures on the shoreface of the wave-dominated Grande-Rivière-de-la-Baleine-delta. *Journal of Sedimentary Research*, 73, 217–226.

20554877, 0, Downloaded from https://onlinelibrary.wiley.com/doi/10.1002/dep2.282 by Readcube (Labtiva Inc.), Wiley Online Library on [14/05/2024]. See the Terms and Conditions (https://onlinelibrary.wiley.com/terms-and-conditions) on Wiley Online Library for rules of use; OA articles are governed by the applicable Creative Commons License

Hjellbakk, A. (1997) Facies and fluvial architecture of a high-energy braided river: The Upper Proterozoic Seglodden Member, Varanger Peninsula, northern Norway. *Sedimentary Geology*, 114(1), 131–161.

Hubbard, S.M., Smith, G.D., Nielsen, H., Leckie, A.D., Fustic, M., Spencer, J.R. & Bloom, L. (2011) Seismic geomorphology and sedimentology of a tidally influenced river deposit, lower Cretaceous Athabasca oil sands, Alberta, Canada. *AAPG Bulletin*, 95, 1123–1145.

Ichaso, A.A. & Dalrymple, R.W. (2009) Tide-and wave-generated fluid mud deposits in the Tilje Formation (Jurassic), offshore Norway. *Geology*, 37, 539–542.

Ichaso, A.A. & Dalrymple, W. (2014) Eustatic, tectonic and climatic controls on an early syn-rift mixed-energy delta, Tilje Formation (Early Jurassic, Smørbukk field, offshore mid-Norway). In: Martinius, A.W., Ravnås, R., Howell, J.A., Steel, R.J. & Wonham, J.P. (Eds.) *From depositional systems to sedimentary successions on the Norwegian continental margin*, Vol. 46, 1st edition. Oxford and Chichester and Hoboken, NJ: IAS Special Publications, pp. 339–388.

Issautier, B., Viseur, S., Audigane, P. & Le Nindre, Y.-M. (2014) Impacts of fluvial reservoir heterogeneity on connectivity: Implications in estimating geological storage capacity for CO_2. *International Journal of Greenhouse Gas Control*, 20, 333–349.

Issautier, B., Viseur, S., Audigane, P., Chiaberge, C. & Le Nindre, Y.-M. (2016) A new approach for evaluating the impact of fluvial type heterogeneity in CO_2 storage reservoir modeling. *Comptes Rendus Geosciences*, 348, 531–539.

Jablonski, B.V.J. & Dalrymple, R.W. (2016) Recognition of strong seasonality and climatic cyclicity in an ancient, fluvially dominated, tidally influenced point bar: middle McMurray Formation, Lower Steepbank River, north-eastern Alberta, Canada. *Sedimentology*, 63, 552–585.

James, N. & Dalrymple, R.W. (2010) *Facies models 4*. St. John's, Newfoundland and Labrador: Geological Association of Canada, p. 586.

Jay, D.A., Talke, S.A., Hudson, A. & Twardowski, M. (2015) Estuarine turbidity maxima revisited: instrumental approaches, remote sensing, modeling studies, and new directions. In: Ashworth, P., Best, J. & Parsons, D.R. (Eds.) *Fluvial-tidal sedimentology*. Amsterdam and Oxford and Waltham, MA: Elsevier. *Developments in Sedimentology*, 68, 49–109.

Keevil, C.E., Parsons, D.R., Keevil, G.M. & Ainsley, M. (2015) Three-dimensional meander bend flow within the tidally influenced fluvial zone. In: Ashworth, P., Best, J. & Parsons, D.R. (Eds.) *Fluvial-tidal sedimentology*. Amsterdam and Oxford and Waltham, MA: Elsevier. *Developments in Sedimentology*, 68, 127–148.

La Croix, A.D. & Dashtgard, S.E. (2014) Of sand and mud: sedimentological criteria for identifying the turbidity maximum zone in a tidally influenced river. *Sedimentology*, 61, 1961–1981.

López-Gómez, J., Alonso-Azcárate, J., Arche, A., Arribas, J., Fernández Barrenechea, J., Borruel-Abadía, V., Bourquin, S., Cadenas, P., Cuevas, J., De la Horra, R., Bienvenido Díez, J., Escudero-Mozo, M.J., Fernández-Viejo, G., Galán-Abellán, B., Galé, C., Gaspar-Escribano, J., Gisbert Aguilar, J., Gómez-Gras, D., Goy, A., Gretter, N., Heredia Carballo, N., Lago, M., Lloret, J., Luque, J., Márquez, L., Márquez-Aliaga, A., Martín-Algarra, M., Martín-Chivelet, J., Martín-González, F., Marzo, M., Mercedes-Martín, R., Ortí, F., Pérez-López, A., Pérez-Valera, F., Pérez-Valera, J.A., Plasencia, P., Ramos, E., Rodríguez-Méndez, L., Ronchi, A., Salas, R., Sánchez-Fernández, D., Sánchez-Moya, Y., Sopeña, A., Suárez-Rodríguez, A., Tubía, J.M., Ubide, T., Valero Garcés, B., Vargas, H. & Viseras, C. (2019) Permian-Triassic rifting stage. In: Quesada, C. & Oliveira, J.T. (Eds.) *The geology of Iberia: a geodynamic approach*. Cham: Springer. https://doi.org/10.1007/978-3-030-11295-0

Lowe, D.R. (1979) Sediment gravity flows: their classification and some problems of application to natural flows and deposits. In: Doyle, L.J. & Pilkey, J.H. (Eds.) *Geology of continental slope*, Vol. 27. Claremore, OK: SEPM Special Publications, pp. 75–82.

MacEachern, J.A. & Pemberton, S.G. (1994) Ichnological aspects of incised-valley fill systems from the Viking Formation of the Western Canada Sedimentary Basin, Alberta, Canada. In: Dalrymple, R.W., Boyd, R. & Zaitlin, B.A. (Eds.) *Incised-valley systems: origin and sedimentary sequences*, Vol. 51. Claremore, OK: SEPM Special Publications, pp. 1–391.

Makaske, B. & Weerts, H.J.T. (2005) Muddy lateral accretion and low stream power in a sub-recent confined channel belt, Rhine-Meuse delta, central Netherlands. *Sedimentology*, 52, 651–668.

Martinius, A.W. & Gowland, S. (2011) Tide-influenced fluvial bedforms and tidal bore deposits (Late Jurassic Lourinha~ Formation, Lusitanian Basin, Western Portugal). *Sedimentology*, 58, 285–324.

Martinius, A.W. & Van den Berg, J.H. (2011) *Atlas of sedimentary structures in estuarine and tidally-influenced river deposits of the Rhine-Meuse-Scheldt System: their application to the interpretation of analogous outcrop and subsurface depositional systems*. Houten: EAGE Publications, p. 298.

Melnyk, S. & Gingras, M.K. (2020) Using ichnological relationships to interpret heterolithic fabrics in fluvio-tidal settings. *Sedimentology*, 67, 1069–1083.

Miall, A.D. (1992) Alluvial models. In: Walker, R.G. & James, N.P. (Eds.) *Facies models response to sea level change*. St John's: Geological Association of Canada, pp. 119–142.

Miall, A.D. (1996) The geology of fluvial deposits. In: *Sedimentary facies, basin analysis, and petroleum geology*. Berlin: Springer, p. 582.

Musial, G., Reynaud, J.Y., Gingras, M.K., Féniès, H., Labourdette, R. & Parize, O. (2012) Subsurface and outcrop characterization of large tidally influenced point bars of the Cretaceous McMurray Formation (Alberta, Canada). *Sedimentary Geology*, 279, 156–172.

Nanson, G.C. & Page, K. (1983) Lateral accretion of fine-grained concave benches on meandering rivers. In: Collinson, J.D. & Lewin, J. (Eds.) *Modern and ancient fluvial systems*, Vol. 6. Oxford and Chichester and Hoboken, NJ: IAS Special Publications, pp. 133–143.

Nemec, W. & Postma, G. (1993) Quaternary alluvial fans in southwestern Crete: sedimentation processes and geomorphic evolution. In: Marzo, M. & Puigdefabregas, C. (Eds.) *Alluvial sedimentation*, Vol. 17. Oxford and Chichester and Hoboken, NJ: IAS Special Publications, pp. 235–276.

Nemec, W. & Steel, R.J. (1984) Alluvial and coastal conglomerates: their significant features and some comments on gravelly mass-flow deposits. In: Koster, E.H. & Steel, R.J. (Eds.) *Sedimentology of gravels and conglomerates*, Vol. 10. Calgary: Memoir. Canadian Society of Petroleum Geologists, pp. 1–31.

Olariu, C. & Bhattacharya, J.P. (2006) Terminal distributary channels and delta front architecture of river-dominated delta systems.

20554877, 0, Downloaded from https://onlinelibrary.wiley.com/doi/10.1002/dep2.282 by Readcube (Labtiva Inc.), Wiley Online Library on [14/05/2024]. See the Terms and Conditions (https://onlinelibrary.wiley.com/terms-and-conditions) on Wiley Online Library for rules of use; OA articles are governed by the applicable Creative Commons License

Journal of Sedimentary Research, 76, 212–233. https://doi.org/10.2110/jsr.2006.026

Olariu, M.I., Carvajal, C.R., Olariu, C. & Steel, R.J. (2012) Deltaic processes and architectural evolution during cross-shelf transits, Maastrichtian Fox Hills Formation, Washakie Basin, Wyoming. *American Association of Petroleum Geologists Bulletin*, 96, 1931–1956.

Page, K. & Nanson, G. (1982) Concave-bank benches and associated floodplain formation. *Earth Surface Processes and Landforms*, 7, 529–543.

Pearson, N.J. & Gingras, M.K. (2006) An ichnological and sedimentological facies model for muddy point-bar deposits. *Journal of Sedimentary Research*, 76, 771–782.

Pham, V.T.H., Halland, E.K., Tappel, I.M., Gjeldvik, I.T., Riis, F. & Aagaard, P. (2013) Long-term behavior of CO_2 stored on a large scale in the Utsira Formation, the North Sea, Norwegian Continental Shelf. *Energy Procedia*, 37, 5240–5247.

Posamentier, H.W. & Walker, R.G. (2006) *Facies models revisited*, Vol. 84. Claremore, OK: SEPM (Society for Sedimentary Geology), Special Publication, p. 527.

Postma, H. & Kalle, K. (1955) Die Entstehung von Trübungszonen im Unterlauf der Flüsse, speziell im Hinblick auf die Verhältnisse in der Unterelbe. *Deutsche Hydrographische Zeitschrift*, 8, 138–144.

Reineck, H.E. (1963) Sedimentgefüge im Bereich der südlichen Nordsee. *Abhandlungen der Senckenbergische Naturforschende Gesellschaft*, 505, 1–138.

Reineck, H.E. & Wunderlich, F. (1968) Classification and origin of flaser and lenticular bedding. *Sedimentology*, 11, 99–104.

Selley, R.C. (2004) *Ancient sedimentary environments and their subsurface diagnosis*. London: Taylor and Francis Group, p. 297.

Shanley, K.W., Mccabe, P.J. & Hettinger, R.D. (1992) Tidal influence in Cretaceous fluvial strata from Utah, USA: A key to sequence stratigraphic interpretation. *Sedimentology*, 39, 905–930. https://doi.org/10.1111/j.1365-3091.1992.tb02159.x

Simons, D.B., Richardson, E.V. & Nordin, C.F. (1965) Sedimentary structures generated by flow in alluvial channels. In: Middleton, G.V. (Ed.) *Primary sedimentary structures and their hydrodinamic interpretation*. Claremore, OK: SEPM Special Publication, p. N.12. https://doi.org/10.2110/pec.65.08.0034

Sisulak, C.F. & Dashtgard, S.E. (2012) Seasonal control on the development and character of inclined heterolithic stratification in a tide-influence, fluvially dominated channel: Fraser River, Canada. *Journal of Sedimentary Research*, 82, 244–257.

Smith, G.A. (1986) Coarse-grained nonmarine volcaniclastic sediment: Terminology and depositional process. *Bulletin Geological Society of America*, 97, 1–10.

Smith, D.G., Hubbard, S., Leckie, D. & Fustic, M. (2009) Counter point bars in modern meandering rivers: recognition of morphology, lithofacies and reservoir significance, examples from Peace River, AB, Canada. *Sedimentology*, 56, 1655–1669.

Soltanian, M.R., Hajirezaie, S., Hosseini, S.A., Dashtian, H., Amooie, M.A., Meyal, A., Ershadnia, R., Ampomah, W., Islam, A. & Zhang, X. (2019) Multicomponent reactive transport of carbon dioxide in fluvial heterogeneous aquifers. *Journal of Natural Gas Science and Engineering*, 65, 212–223.

Sun, X., Cao, Y., Liu, K., Alcalde, J., Cabello, P., Travé, A., Cruset, D. & Gomez-Rivas, E. (2023) Effects of fluvial sedimentary heterogeneity on CO_2 geological storage: Integrating storage capacity, injectivity, distribution and CO_2 phases. *Journal of Hydrology*, 617, 128936. https://doi.org/10.1016/j.jhydrol.2022.128936

Taylor, A.M. & Goldring, R. (1993) Description and analysis of bioturbation and ichnofabric. *Journal of the Geological Society, London*, 150(1993), 141–148.

Tessier, B. & Reynaud, J. (2016) Contributions to modern and ancient tidal sedimentology: an introduction to the volume. In: Tessier, B. & Reynaud, J. (Eds.) *Contributions to modern and ancient tidal sedimentology: proceedings of the tidalites 2012 conference*. Oxford and Chichester and Hoboken, NJ: International Association of Sedimentologists. https://doi.org/10.1002/9781119218395

Thomas, R.G., Smith, D.G., Wood, J.M., Visser, J., Calverley-Range, E.A. & Koster, E.H. (1987) Inclined heterolithic stratification – terminology, description, interpretation and significance. *Sedimentary Geology*, 53, 123–179.

Turner, B.R. & Monro, M. (1987) Channel formation and migration by mass-flow processes in the Lower Carboniferous fluviatile Fell Sandstone Group, northeast England. *Sedimentology*, 34, 1107–1122.

Van den Berg, J.H., Boersma, J.R. & Van Gelder, A. (2007) Diagnostic sedimentary structures of the fluvial–tidal transition zone. Evidence from deposits of the Rhine and Meuse. *Netherlands Journal of Geosciences*, 86, 253–272.

Viseras, C., Fernández, J. & Henares, S. (2011) Facies architecture in outcropping analogues for the TAGI Reservoir. Exploratory interest. AAPG International Conference and Exhibition, Search and Discovery Article, #90135, Milan, Italy.

Viseras, C., Henares, S., Yeste, L.M. & Garcia-Garcia, F. (2018) Reconstructing the architecture of ancient meander belts by compiling outcrop and subsurface data: a Triassic example. In: Ghinassi, M., Colombera, L., Mountney, N.P. & Reesink, A.J.H. (Eds.) *Fluvial meanders and their sedimentary products in the rock record*, Vol. 48. Oxford and Chichester and Hoboken, NJ: IAS Special Publications, pp. 419–444. https://doi.org/10.1002/9781119424437.ch16

Visher, G.S. (1965) Use of vertical profile in environmental reconstruction. *AAPG Bulletin*, 49(1), 41–61.

Yang, B.C., Dalrymple, R.W. & Chun, S.S. (2005) Sedimentation on a wave-dominated, open-coast tidal flat, south-western Korea: summer tidal flat–winter shoreface. *Sedimentology*, 52, 235–252. https://doi.org/10.1111/j.1365-3091.2004.00692.x

Yeste, L.M., García-García, F., McDougall, N.D., Henares, S. & Viseras, C. (2017) Tidal vs fluvial point bars: key features which differentiate them in outcrops, core and wireline logs. 33rd IAS Meeting of Sedimentology, 10–12 Oct 2017, Toulouse, France.

Yeste, L.M., Henares, S., McDougall, N., García-García, F. & Viseras, C. (2019) Towards the multi-scale characterization of braided fluvial geobodies from outcrop, core, georradar and well logs data. In: Corbett, P., Owen, A., Hartley, A., Pla-Pueyo, S., Barreto, D., Hackney, C. & Kape, S. (Eds.) *River to reservoir: geoscience to engineering*. London: GSL Special Publication, p. 488. https://doi.org/10.1144/sp488.3

Yeste, L.M., Varela, A.N., Viseras, C., Mcdougall, N.D. & García-García, F. (2020) Reservoir architecture and heterogeneity distribution in floodplain sandstones: Key features in outcrop, core and wireline logs. *Sedimentology*, 67, 3355–3388. https://doi.org/10.1111/sed.12747

20554877, 0, Downloaded from https://onlinelibrary.wiley.com/doi/10.1002/dep2.282 by Readcube (Labtiva Inc.), Wiley Online Library on [14/05/2024]. See the Terms and Conditions (https://onlinelibrary.wiley.com/terms-and-conditions) on Wiley Online Library for rules of use; OA articles are governed by the applicable Creative Commons License

Yeste, L.M., Palomino, R., Varela, A.N., McDougall, N.D. & Viseras, C. (2021) Integrating outcrop and subsurface data to improve the predictability of geobodies distribution using a 3D training image: A case study of a Triassic Channel–Crevasse-splay complex. *Marine and Petroleum Geology*, 123, 105081. https://doi.org/10.1016/j.marpetgeo.2021.105081

Zweigel, P., Arts, R., Lothe, A.E. & Lindeberg, E.B.G. (2004) Reservoir geology of the Utsira Formation at the first industrial-scale underground CO_2 storage site (Sleipner area, North Sea). *Geological Society of London, Special Publication*, 233, 165–180.

How to cite this article: Yeste, L.M., Gil-Ortiz, M., García-García, F., Viseras, C., Mcdougall, N.D., Cabello, P. et al. (2024) Tidal versus fluvial point bars: Key features from the integration of outcrop, core and wireline log information of Triassic examples. *The Depositional Record*, 00, 1–28. Available from: https://doi.org/10.1002/dep2.282

20554877, 0, Downloaded from https://onlinelibrary.wiley.com/doi/10.1002/dep2.282 by Readcube (Labtiva Inc.), Wiley Online Library on [14/05/2024]. See the Terms and Conditions (https://onlinelibrary.wiley.com/terms-and-conditions) on Wiley Online Library for rules of use; OA articles are governed by the applicable Creative Commons License